MASTERARBEIT | MASTER'S THESIS

Titel | Title

Comparative assessment of PET and collagen vitrigel membranes for in vitro models using NCI-H441 cell line

verfasst von | submitted by

Victoria Ciabuschi BSc

angestrebter akademischer Grad | in partial fulfilment of the requirements for the degree of

Magistra pharmaciae (Mag. pharm.)

Wien | Vienna, 2024

Studienkennzahl lt. Studienblatt | Degree programme code as it appears on the student record sheet:	UA 066 605
Studienrichtung lt. Studienblatt | Degree programme as it appears on the student record sheet:	Masterstudium Pharmazie
Betreut von | Supervisor:	Dr. Carsten Ehrhardt

ABSTRACT

Despite important advances in recent years, the challenges to develop a reliable *in vitro* model able to mimic the complex environment of the human lung remain unmet. The need for an accurate platform able to provide a better predictivity of the potential outcome of pulmonary drug delivery while reducing the use of animal testing is urgent.

In efforts to improve the success of new therapies targeting the lung, this thesis presents an in-depth comparison of Polyethylene terephthalate (PET) and collagen vitrigel membranes for cell culture. Using NCI-H441 cells, a lung adenocarcinoma line, we settled an alveolar epithelium model to evaluate assays that provide key parameters for an adequate blood air barrier model.

Herein, the transepithelial electrical resistance (TEER) was performed to assess the cell monolayer integrity, vital for the development of tight junctions (TJ). Moreover, the permeability of the cell monolayer was evaluated using FITC-labelled dextran of two different molecular masses to examine the transport properties of the membranes. Lastly, the cellular confluency was recorded everyday using a contrast phase microscopy and confirmed with confocal imaging techniques were performed to determine the presence of TJ. All considered, both of the membranes compared proved to be suitable to develop blood air barrier models. Moreover, based on their differences, membranes could have potential applications in different assays.

The results presented herein highlights the successful comparison of two different material-based membranes and their ability to create tight monolayers using alveolar epithelial cells; furthermore, it opens the possibility for more complex in vitro models.

ACKNOWLEDGEMENTS

First and foremost, I would like to extend my profound gratitude to Professor Ehrhardt Carsten, my supervisor, whose role has been fundamental in the realisation of this thesis. Professor Carsten graciously welcomed me into his research group. His unwavering kindness, perpetual enthusiasm, support, and invaluable insights have significantly contributed to the refinement and enhancement of my skills.

I would like to say my thanks to Dr. Mohammed Ali, who helped and advised me along my way.

From the TBSI lab, I would like to thank all PhD students and postdocs; Dr. Fabricio Noel Ledezma Gallegos, Dr. Sean Patmore, Dr. Yashna Chabria, Jean Pierre, Jing Ling, Kris, Mark, Roisin. My experience in Dublin would have not been the same without all of you.

A thank you goes out to the Erasmus + Project Team of Vienna for their support throughout this year and for their funding of my project abroad.

An meine Eltern, Helen, Alessandro und meine Schwester Corinne; ich möchte mich von ganzem Herzen bei euch bedanken. Vom ersten Tag alleine in Wien seid ihr mein moralisches Sicherheitsnetz gewesen. Ohne euch wäre ich nicht so weit gekommen. Der akademische Titel geht auch an euch!

An meine Tante Katrin, Tante Ingrid und Onkel Roberto; eure Ratschläge und Ermutigungen haben mich stets inspiriert. Eure Fürsorge und eure ansteckende Lebensfreude waren für mich eine große Unterstützung und Motivation während dieser Jahre weit weg von Daheim. Der akademische Titel geht auch an euch!

I miei nonni, Arnalda, Giuseppe, Leonilde e Luigi; grazie di tutto, del vostro amore incondizionato, della vostra pazienza, delle vostre parole di conforto e perle di saggezza.

To my girls in Südtirol and Vienna, my second family, the people that saw me growing during those last years. I owe this degree to the unwavering support and non stop encouragement from all of you.

Non temete i momenti difficili.
Il meglio viene da lì.

~ Rita Levi Montalcini

TABLE OF CONTENT

LIST OF FIGURES

LIST OF TABLES

LIST OF EQUATION

ABBREVIATION

ab	Apical-to-basolateral side
AC	Alternative current
AT1	Alveolar type I pneumocytes
AT2	Alveolar type II pneumocytes
ATCC	American Type Culture Collection
ba	Basolateral-to-apical side
BSA	Bovine serum albumin
CLSM	Confocal laser scanning microscopy
CO_2	Carbon dioxide
COPD	Chronic obstructive pulmonary disease
CVM	Collagen vitrigel membran
d_a	Aerodynamic diameter
DAPI	4′,6-Diamidino-2-phenylindole
DMSO	Dimethyl sulfoxide
DPBS	Dulbecco´s Phosphate Buffer
EVOM	Epithelial Voltohmeter
FBS	Fetal Bovine Serum
FITC- dextran	Fluorescein Isothiocyanate-Dextran
h	Hours
HMVEC	Human microvascular endothelial cells
ITS	Insulin-transferrin-sodium selenite
JAMs	Junctional adhesion molecules
KRB	Krebs-Ringer Bicarbonate Buffer
LCC	Liquid covered culture
min	Minutes
O_2	Oxygen
P	p-value
P_{app}	Apparent permeability

PBS	Phosphate-buffered saline
PC	Polycarbonate
PET	Polyethylene terephthalate
PTFE	Polytetrafluoroethylene
RT	Room temperature
SD	Standard deviation
TEER	Transepithelial electrical resistance
TJ	Tight junctions
ZO-1	Zonula occludens-1

CHAPTER 1:

INTRODUCTION

1.1. ANATOMY AND FUNCTION OF THE LUNG

The lungs, located in the chest, is the primary organ of the human respiratory system. The soft and porous tissue that integrates the normal healthy lung gives its elastic characteristics and dynamics [1]. Despite having a complex balance with the cardiovascular system, the lungs function is to supply the body with oxygen (O_2) while eliminating carbon dioxide (CO_2), a metabolic product [1].

The human lung comes in pairs, the right one is subdivided into three lobes, while the left lung has two lobes, with the lower lobe situated next to the heart [2]. Additionally, the respiratory tract can be subdivided into upper and lower tract, each with distinct structures and functions.

The upper respiratory tract consists of the nose, nasopharyngeal cavity, larynx, and glottis. The nasopharyngeal cavity serves for the mechanical cleaning, warming, and humidifying of the incoming air, as well as for immune defence. On the other hand, the function of the larynx is to protect the lower respiratory tract [1]. This continues through the trachea, which bifurcates into two main bronchi; bronchus principalis dexter and sinister. The trachea and the main bronchi together form the conducting zone of the respiratory system and are made of smooth muscle, mucosal lining cells and C-shaped cartilage [4]. The ciliated columnar epithelium with mucus-producing goblet cells not only gives elasticity, but the cartilage prevents the collapse of the trachea during breathing [4].

Following the main bronchi, the lung structure subdivides further into primary bronchi, which then branches into secondary lobar bronchi, and subsequently into tertiary segmental bronchi [1]. Following tertiary segmental bronchi, the air reaches the bronchioles, splitting into conducting, terminal, and respiratory bronchioles.
Within the respiratory bronchioles the gas-exchanging region begins [4]. At this point, the bronchioles are free from the supportive collagen; instead, smooth muscle and elastic fibres are maintaining the anatomical structure together. Mucosal lining can also be found there, with the function of lung protection and to stop exogenous substances from entering the body [4]. Lastly, after 23 generations of bifurcation, the respiratory bronchioles lead into clustered alveoli made of alveolar duct, alveolar

sac, and alveolar capillary [4], [5]. Such an alveoli section is referred to as the respiratory region [6].

The total number of alveoli is estimated to be around 400 million, making up the majority of the lung parenchyma. The alveoli are classified into two different epithelial cell types depending on morphology and function: the squamous alveolar type I (AT1) pneumocytes and the cuboidal alveolar type II (AT2) pneumocytes [7]. AT1 makes up 95% of the alveolar surface [1]. Although AT2 is making the remaining 5% of the area, it is the producer of surfactant, a phospholipoprotein mixture, which is known to decrease the surface tension and prevent the collapse of the alveoli [3].

Neighbouring alveoli are separated by a thin septum and surrounded by a capillary network. The basement membranes of the epithelial and endothelial cells are mostly joined together, creating a very thin barrier through which gases can diffuse [8]. Such barrier is also known as the blood-air barrier. Compounds like collagen, fibronectin, and laminin are found there [9]. The average tissue thickness of the basement membrane is about 0.6 μm, and can be found even thinner in some regions. During gas exchange not only the basement membrane has to be crossed, but also the blood plasma layer, with a thickness of 0.15 μm [1] (Figure 1.1.).

Physiological barriers can be found across the human body. Some examples, next to the above mentioned blood-air barrier, are intestinal-mucosal, dermal, renal-epithelial and blood-brain barrier [10]. As part of this thesis the blood-air barrier is going to be explained more deeply in the next subchapter.

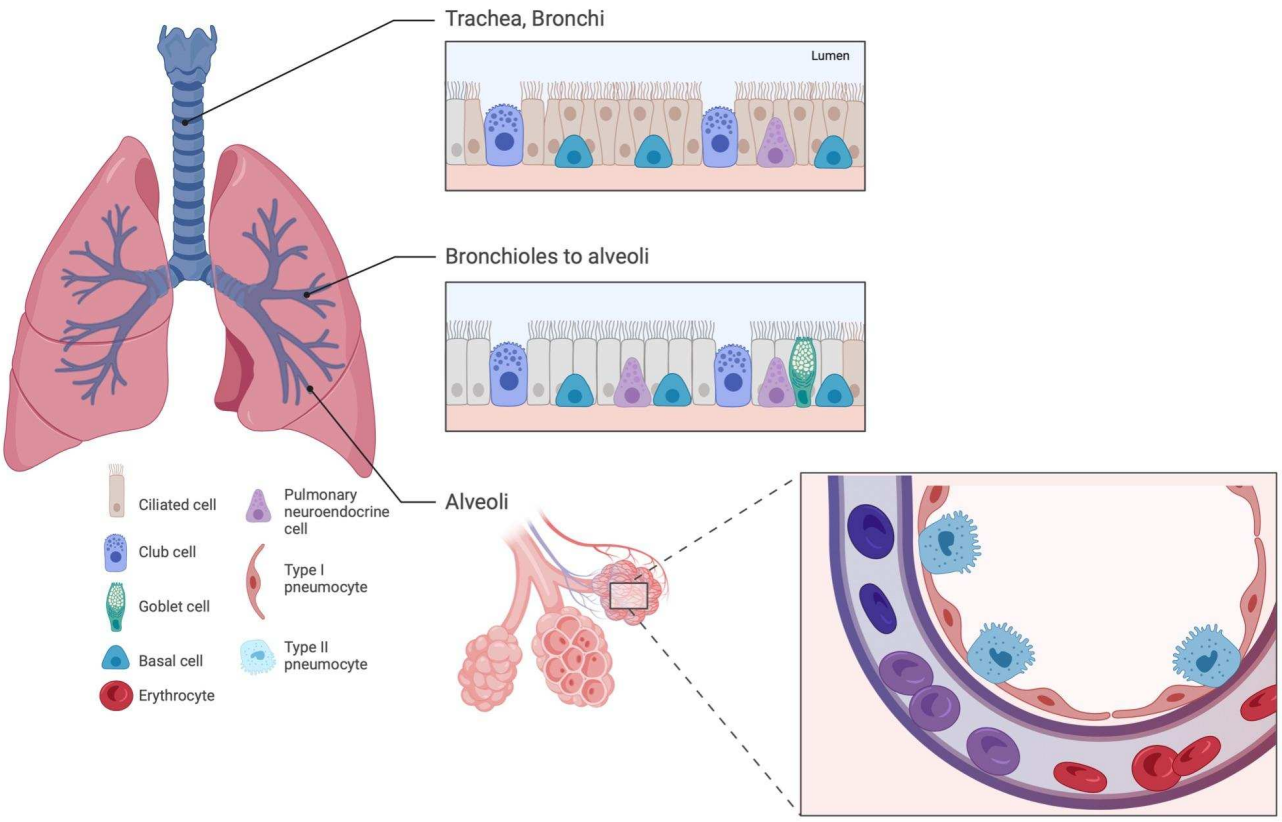

Figure 1.1. Anatomy and epithelial characteristic of the lung in the different lung layers. Adapted from "Respiratory Epithelium" by BioRande.com (2024).

1.1.1. BLOOD-AIR BARRIER

The blood-air barrier of the alveolus is the exchange zone of gases, liquid, and metabolites between blood and inhaled air [10]. CO_2 rich blood arrives from the pulmonary artery to the capillary of the alveoli. While CO_2 diffuses into the alveoli, O_2 on the other side, diffuses into the blood. O_2 rich blood is leaving the alveoli to supply O_2 in the body [1] .

Furthermore, the wellbeing of the barrier determines its function and overall human health [10]. De facto, a barrier deficiency has been linked to serious conditions, such as pulmonary edema. Additionally, the integrity of those barriers are crucial for immune cell migration, metastasis of cancer cells, and nanoparticle transport [9].

In the alveolus epithelial and endothelial cells are tied together via cell-cell junctions, forming a semi permeable diffusion barrier [11]. Cell-cell junctions differentiates from

each other by morphology, composition and function. Nowadays, three different cell-cell junctions are known: adherens junction, tight junction (TJ), and desmosomes.

Because the description of each cell-cell junction would be within the scope of this thesis, the following paragraph will only describe the tight junction in more detail, as these are relevant for further understanding of this work.

TJ or zonula occludens are uninterrupted structures, which circle the lateral membrane of the epithelial cell [7] at the apical pole [10]. TJ's purpose is to supply a physical barrier between apical and basolateral side of endothelial and epithelial membrane, avoiding water, ions and other substances to go through and to keep up cell polarity [7], [10]. Furthermore, TJ also play an important role in cell differentiation, cell growth and proliferation, since they are starting intracellular reactions, which regulates transcriptional pathways [8], [11].

TJ are complexes of different transmembrane proteins, including claudins, occludins, and junctional adhesion molecules (JAMs). However, other TJ parts are also made of peripheral or plaque anchoring protein, as zonula occludens, and TJ-associated proteins [11] (Figure 1.2.).
Those complexes extend around the epithelial cells as a group of intramembrane fibrils, which s also known as 'kissing' points [11]. Additionally, a disturbance of the epithelial barrier can occur in development of inflammation or diseases like chronic obstructive pulmonary disease (COPD) [12].
In response to physiological and pathological stimuli, the intercellular junctions act as dynamic structures that can open or close [13].

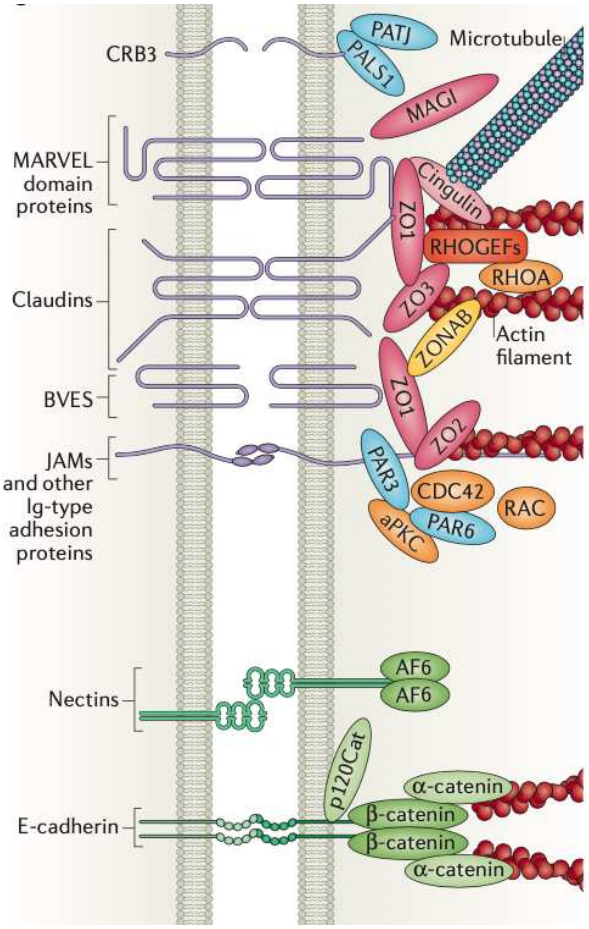

Figure 1.2. Schematic illustration of different TJ subclasses. [14]

1.2. *IN VITRO* MODELS OF PULMONARY DRUG DELIVERY SYSTEMS

Aerosolized inhaled drugs have been used for decades to treat respiratory airway diseases. In the case of COPD, asthma or cystic fibrosis, a local pulmonary drug therapy can be used. Within the last years and the advances in biotechnology, research switched focus from targeting the lung to a more systemic drug delivery. Especially drugs based on proteins and peptides are not only linked with high production costs, but also have a small therapeutic window, needing an efficient delivery to the site of action [10].

The human lung, specially the respiratory zone, with its approximately 120 m² surface area, makes it an ideal drug delivery model [1], contributing also to a systemic effect of the inhaled drug [8]. The alveoli´s barrier not only protects the body from inhaled dust and external pathogens, but also provides an entry point for inhaled drugs. Furthermore, the low enzymatic activity and 5 L/min floating blood into the alveoli, makes the systemic effect easier [5],[8].
Drugs entering the blood system in this way, are overcoming the first pass effect of the liver and respond to lower side effects, making this type of delivery system engaging [5],[6].

The transport across the lung and deposition of inhaled drugs is determined not only by the respiratory tract morphology and breathing pattern [15], but also by parameters such as aerodynamic properties of the aerosol, its particle size, shape, and density.
The aerodynamic diameter (d_a) stands as the foremost parameter for evaluating the optimal targeting of therapeutic aerosol particles. d_a is calculated by multiplying the particle's geometric diameters and the square root of the particle's mass density [5].
Particles having an d_a over 6 µm stays in the upper airways, instead particles with the d_a size between 2 and 6 µm are best suited for local therapy on the lung. When a systemic effect is wished, a d_a between 2 and 3 µm is aimed, because those reach the alveolar region [8]. Particles with d_a < 1µm will impede deposition, leading to their exhalation [5].
In the epithelial lining fluid, a drug with high water solubility can readily dissolve and be promptly absorbed. On the other hand, the dissolution rate might become the limiting factor for more hydrophobic substances. The primary challenge for inhaled drugs to attain their pharmacological targets is thought to be their uptake across the lung epithelial barrier. [16].

Drugs can be absorbed in three different ways; 1) passive diffusion 2) endocytosis with help of vesicles or transcytosis, and 3) transporter-mediated uptake or efflux [2] (Figure 1.3.).
Small lipophilic drugs use passive diffusion to go through the cell membrane, hydrophilic substances on the other hand are absorbed by the last two ways. However a diffusion through the TJ pores is also possible for hydrophilic drugs [6] .

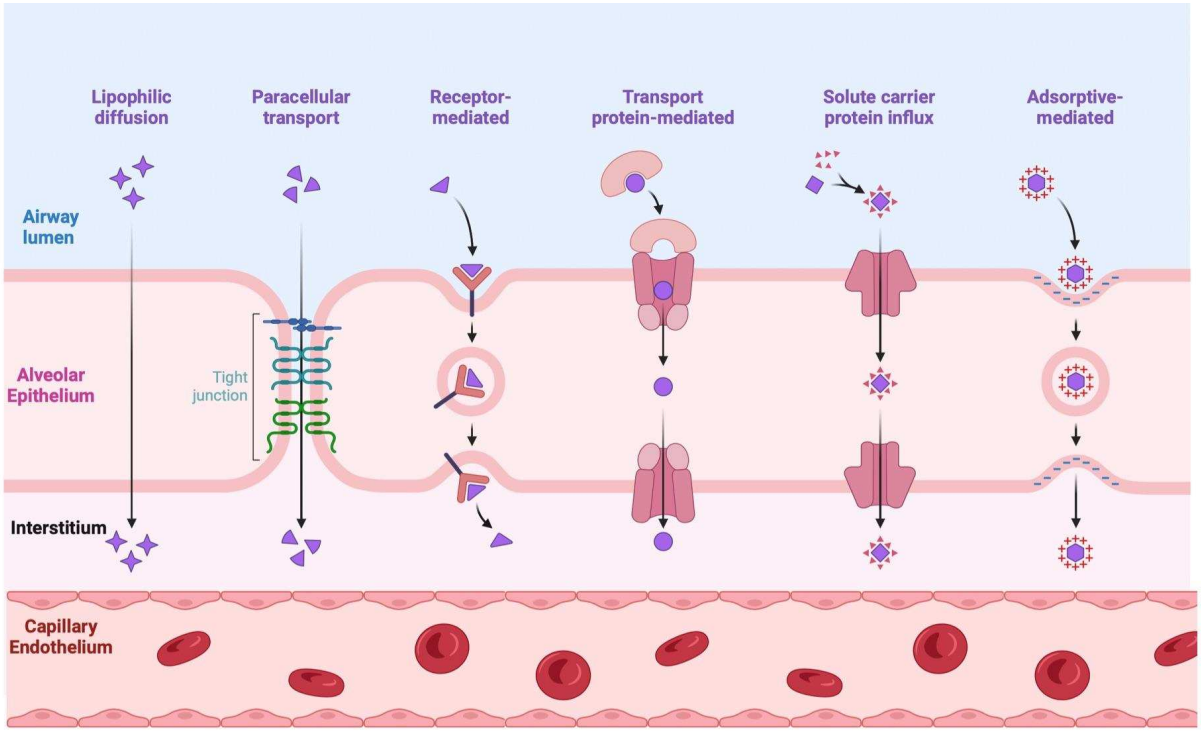

Figure 1.3. Absorption pathway in the alveolar epithelium. Adapted from "Solute Transfer Across Blood-Brain Barrier" by BioRander.com (2024).

In recent years, an increasing development of reliable *in vitro* and *ex vivo* model systems that replicate the functions of the human lung for use in preclinical drug development and safety testing has been observed [8],[2].
The refinement of *in vitro* barrier models to act like *in vivo* models would bring an increase to the predictability of pharmacokinetics and pharmacodynamics of tested substances [17].

This progress has been motivated not only by the commitment to adhere to more ethical practice in animal testing, but as cases of lung related diseases are increasing, improvement for precise medicine drive for pulmonary barrier research [2]. Next to cost-wise advantages, a precise dose and defined drug concentration can be used when working with *in vitro* models. Furthermore, the variability in culture is reduced *in vitro* over *in vivo* models. They are also widely more accepted than *in vivo* animals, because of their higher and quicker throughput possibility [17].

In vitro models have been the gold standard in the market for epithelial human lung barrier with options such as simple continuous cell lines on plastic membrane, multi cell co-culture models, and 3D cultures [8],[18]. Additionally, pulmonary tissue isolated from humans, perfused lungs, or lung lobes can be found.
Moreover, the number of cell types considered for lung models for human blood-air barrier has increased, though, not all successful [19]. Biopharmaceutical studies are using primary cells isolated at the moment from patients, as well as continuously testing cancer or immortalised cells [8].

Thus the importance of establishing a blood air barrier model that mimics the *in vivo* setting and is reliable for biopharmaceutical studies, the ability of cells to form a polarised confluent single layer with functional cell-cell junctions is vital [20]. Due to this, the permeability and integrity of cell monolayer has become a key parameter for determining the suitability of a cell model [8].

Integrity and permeability assays involve the seeding of cells in transwells, also known as inserts, that have, on the bottom end, a nano- or microporous membrane. Cells can then be cultured under liquid-covered culture (LCC) or air-liquid culture (AIC) conditions [15].

When cultured under appropriate conditions, cells can differentiate, retain their morphology and metabolism as well as secret surfactant or mucus. Besides, cell processes like ciliogenesis, expression pathways, membrane transporters and metabolic enzymes follow a normal behaviour [18]. However, over a long period in culture, such characteristics can be lost due cell phenomena like transdifferentiation and dedifferentiation [19].

All considered, the cell line NCI-H441 has been an established model for epithelial barrier. NCI-H441 is an immortalised cell line; one of the few able to form an electrically tight monolayer of polarised cells. Besides, recents studies found that it is a suitable primary cell substitute for ion and drug transport [8].

NCI-H441 cells were originally obtained from a caucasian male with papillary adenocarcinoma in 1982. The cell line is used as a model of human alveolar

epithelial lun as it shows similarity to a club cell like epithelium [8] and ATII parenchyma [16]. Furthermore, they express markers of AT1 and AT2 cells [8].

Studies have shown that NCl-H441 can reach TEER values of 1000 Ωcm^2 after 13 days in culture, with adequate seeding density and media supplements [21] .

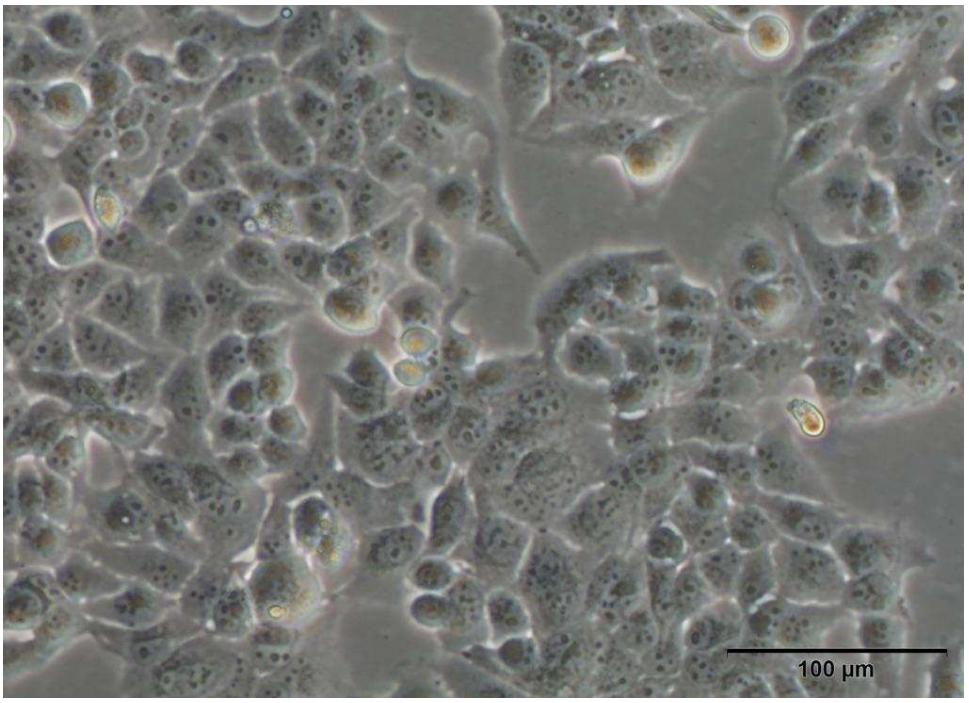

Figure 1.4. NCl-H441 cell line in a T75 flask.

In vitro models are adapting different technologies, for instance, inserts for assessing drug diffusion through the blood-air barrier or other studies.

Inserts can be broadly divided in 3 classes: polycarbonate (PC), polyester (PET), and collagen-coated polytetrafluoroethylene (PTFE) [22]. Since the objective of this project is to compare the PET and collagen vitrigel inserts based on their ability to improve cell growth and attachment parameters, their characterisation and technical specifications are going to be described in this subchapter.

From chapter 2 to 5, the two different membranes are going to be referred to as PET and collagen vitrigel membrane (CVM). Nonetheless, it's important to mention that

the commercial name of the PET membrane was Transwell®-Clear Insert (#3470, Corning®). On the other hand, for the CVM tranwells, the Ad-MED Vitrigel™ 2 (#08364-96, Kanto Chemical Co.,INC.) was used.
Additionally, numbers above referring to the transwells are based on a 24 well plate, since those were the size purchased.

1.2.1. Ad-MED Vitrigel™ 2 TECHNOLOGY

Takezawa and colleagues at the National Institute of Agriculture and Biological Resources created the collagen vitrigel technology. The collagen is made of high density collagen fibres [23], which is claimed to be analogous to *in vivo* connective tissue, showing high transparency, mechanical stability, and permeability for proteins. Membrane porosity is low due to the vitrification process, thickness wise, it is claimed to be >10 μm [6]. Ad-Med Virtigel™ 2 is a cell culture insert, which includes collagen vitrigel feature [24].

Kanto Chemical Co.,INC. describes on their website the process of vitrification to produce the membranes, as follows: firstly a drying process removes the moisture, like water, from the collagen gel. Due to the increased density of collagen fibres, collagen gel turns into a film, called “vitrigel” [25] (Figure 1.5). Bright field microscopy reveals a uniform small grain pattern from the collagen vitrigel (Figure 1.7.) [26].

Although collagen-based materials have been used already for a long period in medicine and in cell culture, the collagen used in the transwells had different properties. Because of its white colour, microscopy observations over treated areas were difficult to carry out. They also needed additional chemicals, like plastic and cross-linking materials.

Collagen vitrigel, on the other hand, depicts a different set of characteristics.

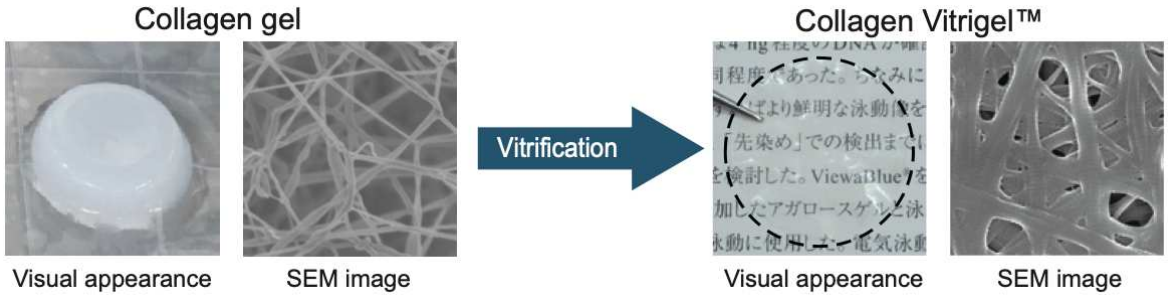

Figure 1.5. Vitrification Process and SEM Images [25].

1.2.2. TRANSWELL®-CLEAR INSERT

Transwell®-clear inserts were obtained from Corning. They present a membrane made of PET, having a pore size of 0,4 µm.

This type of semi permeable membrane is offered in different pore sizes; the range goes from 0,4 to 8 µm. When creating a barrier model, cells are cultured commonly on one side of the membrane. Generally speaking the smallest pore size is going to be used for permeability studies, while bigger pore sizes are suitable for migration studies [9].
The thickness of a PET membrane is approximately 10-12 µm, making it bigger than the basement membrane found *in vivo*. Nonetheless, PET inserts are used for mimicking basement membrane in *in vitro* studies [9]. This physical threshold blocks cell-cell contact across the membrane and limits transport of substances between cells [9].

Furthermore, bright field microscopy shows a non uniform grain pattern [26] (Figure 1.6.), needing no additional chemicals and presenting no optical problems because of its transparent nature [23].

Table 1.1. Comparison of technical specification of two used membranes. Data taken from suppliers website [27] [25].

Transwell®-Clear Insert	**Technical specification**	**Ad-MED Vitrigel™ 2**
Polyethylene terephthalate (PET)	Material of the membrane	Collagen vitrigel membrane with a high-density collagen fibre
0.33 cm²	Membran area	0.33 cm²
0,4 µm	Pore size	Matrix (non specified)
$4x10^6$ pores per cm²	Pore density	
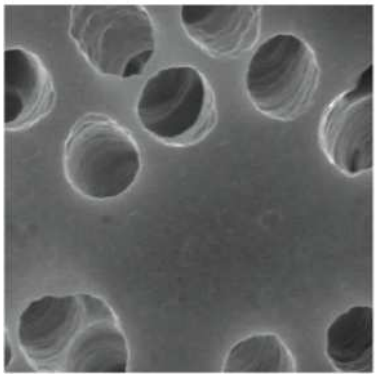	SEM Images	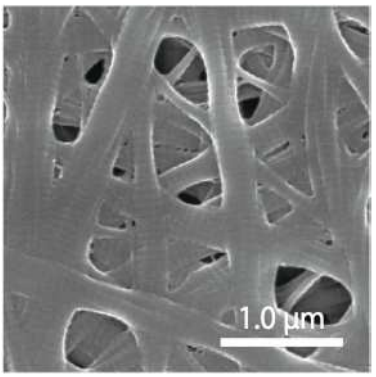
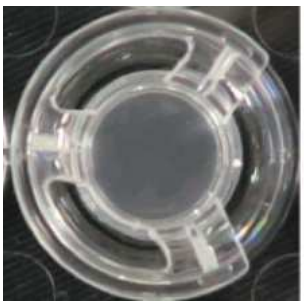	Structure	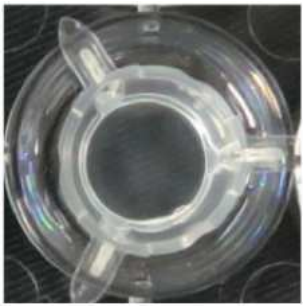

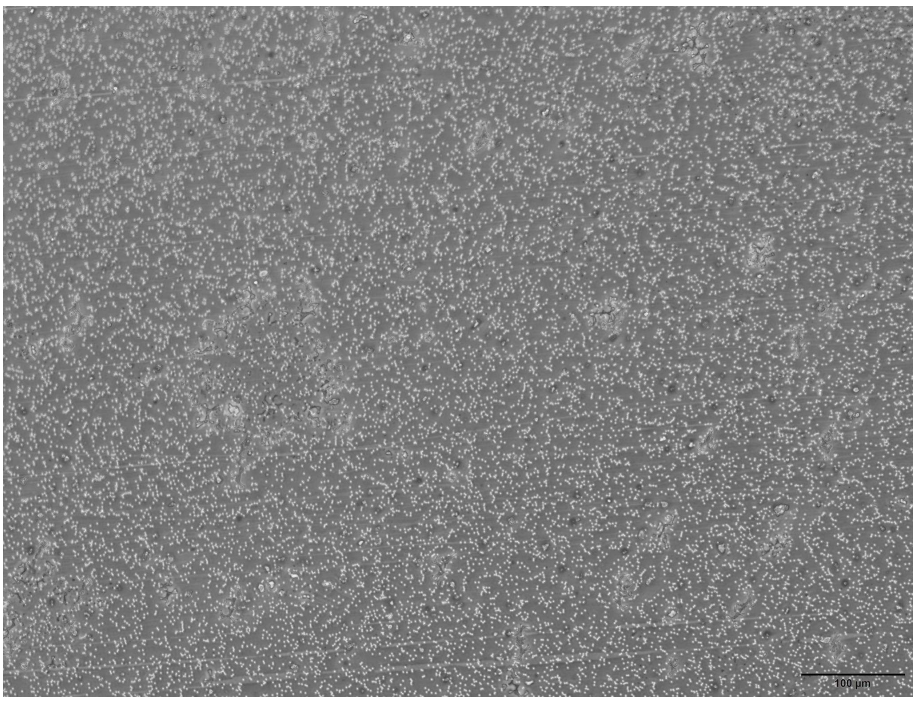

Figure 1.6. 10X Bright field microscopy image of PET membrane without cells.

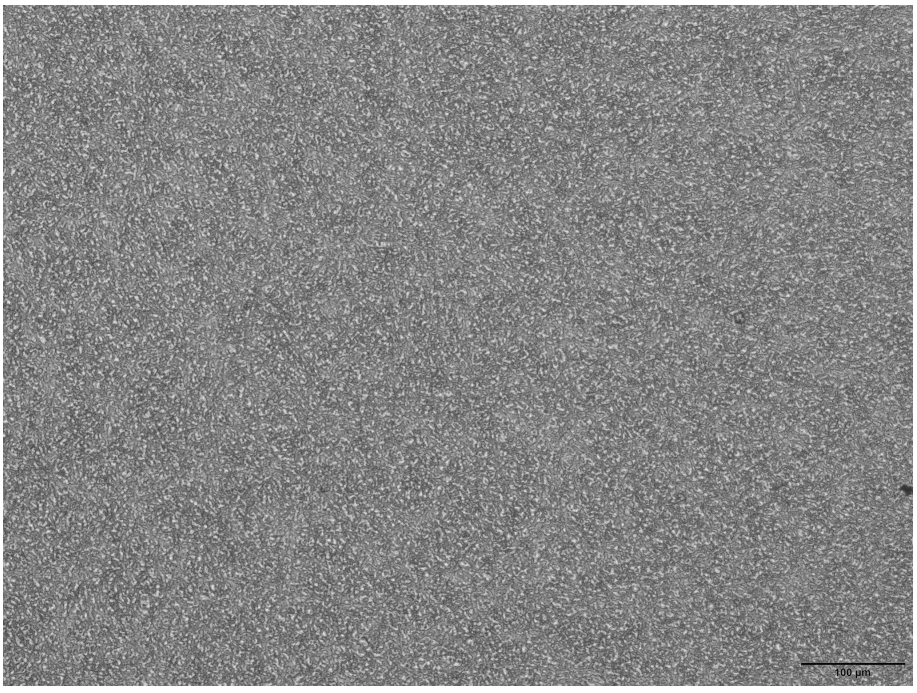

Figure 1.7. 10X Bright field microscopy image of CVM membrane without cells.

1.4. OBJECTIVES

The primary aim of this thesis is to systematically compare the efficacy of two different transwell insert membranes. One composed of PET while the other presents collagen vitrigel.

Comparative analyses will include the growth and functionality support of NCI-H441 cells, specifically focusing on the expression and structural integrity of tight junctions. These assessments are crucial for understanding the suitability of these membrane materials in simulating the human alveolar epithelium; essential for the testing of pulmonary-targeted drug delivery systems. The following objectives outline the rationale behind the selection of specific methods used in this research.

1.4.1. EVALUATION OF MEMBRANE INTEGRITY USING TEER

The integrity of the cell membrane is a critical factor in determining the suitability of a model to simulate the alveolar barrier in humans. TEER measurements provide a non-invasive, quantitative indication of the tightness of the cell barrier in culture models, correlating values directly to the presence and integrity of the tight junctions between cells. High TEER values typically indicate robust barrier properties, which are vital for maintaining selective permeability crucial in lung function and drug delivery.

1.4.2. ASSESSMENT OF PERMEABILITY USING FITC-LABELLED DEXTRAN

Permeability studies are a cornerstone of evaluating transwell systems for drug transport evaluations. In this thesis, the permeability of the two membrane types to FITC-labelled dextran molecules of various sizes was analysed. The ability of the membranes to modulate the cross of these molecules can shed light on the potential efficacy of drug delivery applications, where molecular transport is essential.

1.4.3. ANALYSIS OF TIGHT JUNCTION FORMATION USING CONFOCAL LASER SCANNING MICROSCOPY

Lastly, CLSM was used to obtain precise insights into the structural formation and development of TJ in NCI-H441 cells over time. By conducting CLSM at three pivotal times, the study seeks to document the dynamic changes in TJ formation and integrity. The evaluation through time aims at determining the membrane support to cellular differentiation and function during the time of the study..

CHAPTER 2:

MATERIALS AND METHODS

2.1. CELL CULTURE

2.1.1. MAINTENANCE OF CELL LINE NCI-H441

The NCI-H441 human epithelial pulmonary papillary adenocarcinoma cell line (ATCC HTB-174) was obtained from LGC Promochem (Teddington, UK) and continuously maintained in 75 cm2 culture flasks (Greiner BioOne, Frickenhausen, Germany) at 37 ºC and 5% CO2 in a humidified incubator (Binder MODEL/COUNTRY NEEDED).

For cell growth, a standard medium, consisting of RPMI 1640 (Gibco, Biosciences, Dun Laoghaire, Ireland) supplemented with 5% foetal bovine serum (FBS) (v/v) (Sigma-Aldrich, Arklow, Ireland), 1% sodium pyruvate (v/v) (Sigma-Aldrich, Arklow, Ireland), and 1% penicillin/streptomycin (10,000 units penicillin and 10 mg/mL streptomycin) (v/v) (Sigma-Aldrich, Arklow, Ireland), was used and changed every other day.

Above mentioned conditions will be referred subsequently as “standard medium” and “standard conditions”.

2.1.2. PASSAGING CELL NCI-H441

Subculture of cells was carried out when the confluence reached 80-90%. The passage procedure consisted of discarding the medium followed by washing the cell monolayer with Dulbecco’s phosphate-buffered saline (DPBS) (Sigma-Aldrich, Arklow, Ireland). Then, the DPBS was replaced with 1x trypsin-EDTA solution (Sigma-Aldrich, Arklow, Ireland) and the flasks were incubated under standard conditions until the cells were detached (3 to 5 min). Any remaining trypsin was deactivated by FBS (Sigma-Aldrich, Arklow, Ireland) in fresh, pre-warmed culturing media. The cell suspension was transferred to 50 mL plastic tubes (Corning, NY, USA) and centrifuged at 900 rpm for 5 min at room temperature (RT) (Centrifuge 5810 R, Eppendorf); 200 µL were taken for cell counting. Finally, the supernatant was aspirated and the cell pellet was resuspended in fresh medium; depending on

the confluence requirements, seeding ratios of 1:10 - 1:5 were subcultured in new flasks.

When seeding for biological replicates of experiments, similar seeding densities were used to ensure consistent growth times.

2.1.2.1. CELL COUNTING USING A HEMOCYTOMETER

The number of cells was determined using a hemocytometer from 200 µL aliquots. The procedure consisted of placing 10 µL of cell suspension on both chambers of a previously cleaned hemocytometer using a coverslip. Cells were counted using a microscope with a 10X objective and a hand tally counter. To determine the number of cells per mL present in the cell suspension, the average count of the four sets of the 16 corner squares was multiplied by 10,000, as expressed in the following equation:

$$original\ cell\ suspension\ [cell/ml] = \frac{Number\ cell\ counted}{Number\ of\ corner\ square\ sets} * 10.000$$

Equation 2.1. Determination of cell number using a hemocytometer

2.1.3. CRYOPRESERVATION & THAWING OF NCI-H441 CELL LINE

2.1.3.1. CRYOPRESERVATION OF NCI-H441 CELL LINE

The NCI-H441 cells were routinely maintained and passsaged as explained in 2.1.1 and 2.1.2. After determining the cell count, 2 x 10^6 cells were resuspended dropwise in 1 mL freezing medium, consisting of 90% of standard medium supplemented with 10% of dimethyl sulfoxide (DMSO) (Sigma-Aldrich, Arklow, Ireland) suitable for cell culture. The cell suspensions were swiftly transferred to cryovials, immediately placed in a Mr. Frosty freezing container (Thermo Fisher Scientific), and frozen at −80 °C for 48 h before transferring them to a liquid nitrogen container for long-term storage.

2.1.3.2. THAWING OF NCI-H441 CELL LINE

The cell revival procedure consisted of removing cryovials stored in liquid nitrogen and placing them in a water bath at 37 ºC until partial defrost of the cell suspension. Immediately after complete thawing, the cell suspension was transferred to a 15 mL plastic tube and mixed with a pre-heated standard medium to a final volume of 5 mL. Following, the sample was centrifuged at 900 rpm for 4 min at RT, the supernatant was discarded, and the cells were resuspended in standard medium or enriched medium with 10% FBS. The fresh cell suspension was initially cultured in 25 cm^2 flasks and at least two passages were performed before their use in experiments.

2.2. TRANSWELL CLEAR INSERTS

Throughout the project's duration, two types of 24-well transwell clear inserts were utilised: CVMel™ 2 (#08364-96, KANTO CHEMICAL CO., INC) and Transwell®-Clear Inserts with Polyester (PET) membrane (#3450, 0.4 µm pore size, Corning, Bedford, MA).

2.2.1. COATING OF TRANSWELL CLEAR INSERT

While the Ad-MED Vitrigel™ 2 inserts have a collagen membrane made by the manufacturer, the Transwell®-Clear inserts were treated with collagen in the laboratory before their use in every experiment performed during this research project.

The Transwell-Clear inserts were coated with 25 µg/cm^2 of rat-tail collagen type I (#A10483-01, Thermo Fisher Scientific). The required concentration of collagen was calculated and diluted in serum-free RPMI 1640 media with 1% sodium pyruvate. Equal volume of the mixture was added to each apical side of the transwell and incubated under standard conditions overnight. Then, the coating was removed and the transwells were washed with PBS and left to dry for 30 min in a laminar flow cabinet. Subsequently, the plate containing the coated filter was wrapped in parafilm and stored at 4 ºC for a maximum of two weeks. Before cell seeding, standard media

was added into both apical and basolateral compartments, followed by a 30-min incubation at 37ºC.

2.2.2. CELL SEEDING ON TRANSWELLS

For all experiments, a seeding density of 100,000 cells/cm² was employed. Clear 24-well transwell inserts were used: Ad-MED Vitrigel™ 2 (#08364-96, pore size 1.0 µm, KANTO CHEMICAL CO., INC) and Transwell®-Clear Inserts with Polyester (PET) membrane (#3450, pore size 0.4 µm, Corning, Bedford, MA).

Cells were maintained as described in section 2.1.2 and seeded in standard medium supplemented with 1 µM dexamethasone (Thermo Fisher Scientific) and 1% insulin-transferrin-sodium (ITS premix universal culture supplement; Corning).

For optimal cell distribution and uniform monolayer formation in the transwells, the seeding volume was halved compared to that recommended by the supplier's datasheet. Subsequently, the volume was restored to the recommended volume.

For all experiments, a seeding density of 100,000 cells/cm² was employed.

2.3. MONOLAYER INTEGRITY ASSESSMENT

To assess monolayer integrity, measurements of transepithelial electrical resistance were conducted.

2.3.1. TRANSEPITHELIAL ELECTRICAL RESISTANCE

In order to determine the transepithelial electrical resistance, 100,000 cells/cm^2 were seeded per transwell in the two types of transwells. After 48 h, the standard medium was replaced with growth medium supplemented with 1 µM of dexamethasone and 1% insulin-transferrin-selenious. The cells were cultured under liquid-covered culture (LCC) conditions, consisting of 0.6 mL on the basolateral side and 0.1 mL on the apical side. Media was renewed every other day.

From days 3 to 13, the integrity and the ability of cells to form electrically tight junctions were assessed by measuring the transepithelial electrical resistance (TEER) values using a Millicell ERS-2, EVOM2™ voltohmmeter and EVOM STX4 Electrode (Millipore, Carrigtwohill, Ireland). Since temperature is known to affect the stability of the TEER readings, the plates were taken out of the incubator for 15 min before the analysis. All values were recorded in triplicate.

The following equation was used to determine the net TEER value:

$$TEERnet = (TEERraw - corrective\,value) * A$$

Equation 2.2. Determination of the transepithelial electrical resistance value. Corrective Value = 100Ω; A (surface area of 24-well transwell) = 0.33cm^2.

2.4. PERMEABILITY STUDY

The permeability of the cell monolayer was determined by seeding 100,000 cells/cm^2 per transwell in both types of transwells. After 48h, the standard media was substituted with fresh supplemented with ITS premix universal culture supplement. The cells were then cultured under LCC conditions, with 0.6 mL of media added to the basolateral side and 0.1 mL to the apical side. Media changes were carried out every other day.
TEER values were also assessed both before and after experiments to evaluate the integrity of the cell barrier.

The study was conducted when TEER values exceeded 500 Ωcm^2.
On the day of the experiment, the medium in the inserts was removed and cell monolayers were rinsed with Krebs-Ringer Bicarbonate Buffer (KRB) and subsequently allowed to equilibrate in KRB at 37 °C for 1 h.
After incubation time, two compounds were tested to determine the permeability of the cell monolayer: FITC-dextran of molecular weight 4000 (4K) and FITC-dextran of molecular weight 20.000 (20K) (Sigma-Aldrich, Arklow, Ireland). Both polymers were diluted in KRB at a concentration of 1 mg/mL.

The following volumes were used in both transwell clear inserts:

Apical to basolateral (ab), 25 mL of donor solution was added to the apical side, while 0.8 mL of KRB was added to the basolateral side.

Basolateral to apical (ba): 0.85 mL of donor solution was added to the basolateral side and 0.2 mL of KRB was added to the apical side.

Immediately after the addition of the donor fluid, 50 µL samples were collected from the donor side to determine initial concentrations. Plates were then incubated at 37 °C for 90 min; 100 µL samples were taken from the acceptor side every 15 min. The removed volumes were immediately replaced with fresh KRB to maintain equilibrium. At the end of the experiment, 50 µL of the acceptor side was collected.

The fluorescence intensity of the samples was analysed in 96-well plates using an automated plate reader (FLUOstar Optima, BMG Labtech, Offenburg, Germany) configured to excite the samples at a wavelength of 485 nm and detect emission at 520 nm.

Apparent permeability coefficient (P_{app}) was calculated by following equation;

$$Papp = \frac{\frac{\Delta Q}{\Delta t}}{A * C0}$$

Equation 2.3. Determination of the apparent permeability coefficient.

ΔQ represents the change in the concentration of FITC-dextran over a period of time (*Δt*). *A* denotes the area of the transwell clear insert, while *C0* expresses the initial concentration of FITC-dextran in the donor solution.

2.5. CONFOCAL LASER SCANNING MICROSCOPY

NCI-H441 cells were seeded at a density of 100,000 cells/cm^2 per transwell in both sets of transwell clear inserts. Subsequently, the cells were cultured for 48h, 6 days, and 12 days.

The samples were then washed twice with a solution of PBS supplemented with 1% bovine serum albumin (BSA) (v/v) (Sigma-Aldrich, Arklow, Ireland) and 0.05% Tween 20 (v/v) (Sigma-Aldrich, Arklow, Ireland). The volumes used were as follows: apical space 200 µL and basolateral space 800 µL. Then, two additional washes of the inserts with PBS (both inside and outside) were performed.

All further steps and volumes refer to the apical chamber.

Following washing, the cells were fixed with 200 µL of 2% paraformaldehyde (PFA) in PBS (w/v) for 7 min. Following, PFA was neutralised by blocking with 200 µL of 50 mM NH_4Cl for 10 min.

Cells were then permeabilised with 200 µL of 0.1% Triton X-100 in PBS (v/v) for 8 min, followed by blocking with 200 µL of 2% BSA in PBS (w/v) for 45 minutes.

Following, the cells were incubated overnight at 4 °C with 50 µL of primary antibodies diluted in 1% BSA in PBS (w/v) as specified in Table 2.6.

On the following day, the cell monolayers were washed by adding 1% BSA in PBS (further on in this section referred as washing buffer) for 15 min; this step was repeated three times. Then, cells were incubated with 50 µL of Alexa Fluor 594-conjugated secondary antibody diluted in PBS containing 1% BSA (w/v) (as specified in table 2.6.) for 1 hour at 37°C.

Antibodies were removed and cells were washed for 20 min with washing buffer. Following, cell monolayers were incubated with 100 µL of Hoechst 33342 solution (1 µg/ml in PBS) for 15 minutes for nuclei counterstaining.

After two cycles of washing buffer of 20 min each, the transwell inserts were carefully cut out using a scalpel blade and transferred onto a microscope slide. To mount the filters, a drop of Ibidi mounting medium (Ibidi, Germany) was added to the slide, followed by attaching the sliced transwell with the cells facing upwards. An additional drop of FluorSave was added onto the slice and a cover slip was mounted on top of the sample.

Finally, the samples were allowed to dry in a cool, dark place for at least one hour before analysis. Visualisation of the samples was conducted using a Leica SP8 confocal laser scanning microscope equipped with a 20X dry objective (Leica).

Table 2.1. Primary and secondary antibody for confocal scanning laser microscopy

Type of Ab	Antibody name (catalog no.)	dilution factor
1st	Rabbit monoclonal anti-ZO-1 Ab (Cell Signaling #13663)	1:100
2nd	Goat anti Rabbit IgG Alxa Fluor 594 (ThermoFischer #A11072)	1:500

2.6. STATISTICAL ANALYSIS

The statistical methods applied in this thesis were one-way analysis of variance (ANOVA) followed by Bonferroni comparisons using the GraphPad Prism version 8.6 (La Jolla, CA, USA). All results are presented as mean ± standard deviation (SD). The levels of significance are: *$p<0.05$, **$p<0.01$, ***$p<0.001$.

CHAPTER 3:

RESULTS

3.1. MONOLAYER INTEGRITY - TRANSEPITHELIAL ELECTRICAL RESISTANCE

In order to determine integrity of the cell monolayer, assessments were carried by determining the transepithelial electrical resistance values.

Overall, TEER values in both types of transwells depicted an increase throughout the experiment. The two transwells showed a similar increment after one day of incubation, going to 113.4 ± 23.06 Ωcm^2 for PET and 144.4 ± 24.61 Ωcm^2 for CVM. Nonetheless, from day 5 to 9 the values did not show much variation. It is important to mention that such values were different in the two transwells, being the CVM ones the maintained higher values in a range of 181.9 ± 31.27 Ωcm^2 to 205.5 ± 28.28 Ωcm^2, as compared to the PET, which recorded a range of 130.4 ± 35.73 Ωcm^2 to 152.6 ± 36.50 Ωcm^2, resulting in statistical significance on days 8 and 9, with ***$p<0.001$. This trend is in line with the high percentage of cell confluence observed.

During day 10, the TEER values of both inserts followed a similar drop, reaching the lowest values of the study, with 73.54 ± 15.05 Ωcm^2 in CVM and 80.41 ± 16.23 Ωcm^2 in PET. Throughout day 10 to 13, the TEER measurements showed minor changes, only describing a slight increase at day 12 with values of 106.7 ± 17.39 Ωcm^2 and 100.5 ± 19.85 Ωcm^2 for CVM and PET respectively.

TEER values in both transwell inserts increased between day 3 to 5, stabilising till day 9 and then decreasing after that.
On day 7, H441 cells were reaching their highest confluency with 152 ± 36.50 Ωcm^2 for PET and 197.7 ± 20.44 Ωcm^2 for CVM (Figure 3.1.1.). CVM in contrast to PET shows higher TEER values from day 5 to 9. Although, a statistical difference between TEER values of the two transwells was determined only on day 8 and 9, with ***$p<0.001$.

On the other days no significant difference was observed.

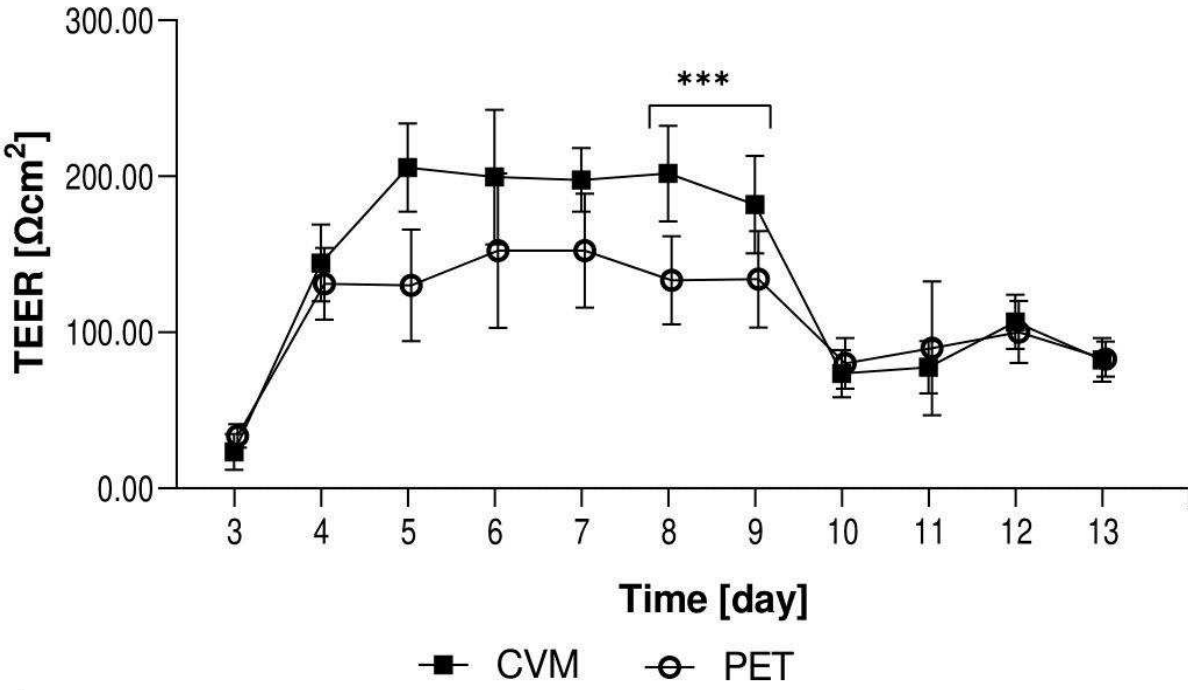

Figure 3.1. TEER measurement in NCI-H441. Cells were seeded and TEER measurements were recorded on days 3 to 13. Comparative analysis was performed between PET and CVM Transwell inserts. Values represent mean measurements of at least 3 individual replicates ± SD. Statistical significance: ***p<0.001.

3.2. PERMEABILITY STUDY

Once the TEER values were determined and linked to the cell confluency in the inserts, a permeability study was carried out to further investigate the integrity of the cell monolayer. For this purpose, two polymers were used: FITC-dextran 4 kDa and a more complex 20 kDa. Furthermore, two sets of experiments were performed with each one of the FITC-dextran; an initial one where the migration occurred from the apical side to the basolateral while a second one was performed where the opposite molecule movement was analysed.

When the cell monolayer was exposed to FITC-dextran 4 KDa on the apical side (Figure 3.2. A), a clear difference was observed in the permeability between the two types of inserts. The CVM inserts followed a sustained increase, starting with a mean concentration of 0,1542 ± 0,07241 mg measured at 15 min and reaching a

maximum diffusion of 0,35441 ± 0,1047 mg at the last time point. In contrast, the PET depicted a statistically significant lower permeability, resulting in an initial amount of 0,05083 ± 0,0176 and finalising at 0,08950 ± 0.03881. These results represented a transport percentage of 129% and 76% respectively.

When the FITC-dextran 4 kDa was analysed in the basolateral side (Figure 3.2. B) of the CVM inserts, an increasing transport trend was observed. The recorded mean amount of the polymer at 15 min was 0,09431 ± 0,1045, going up to 0,3723 ± 0,1693 at 90 min, which represents 295% increment. However, while the PET also followed an increasing transport trend, a flattening of the curve was noted after 45 min, with minor changes registered. Such type of transwell showed lower permeability than its counterpart, reading 76% increase after 90 min.

Then, the ability of FITC-dextran 20 kD to cross the cell monolayer was assessed. Initially, the polymer was added on the apical side to analyse its movement to the basolateral portion (Figure 3.2. C). Herein, both types of inserts illustrated a time-dependent increase of the transported polymer, similarly to the pattern observed in the FITC-dextran 4 kDa experiment. Moreover, a marked difference was observed between the two transwells. The CVM showed a statistically significant higher amount of transported FITC-dextran in all the time-points analysed. The largest difference recorded was after 90 min, when the fluorescent polymer amount in the basolateral side of the CVM transwells was 6.6 fold higher than that in PET.

Finally, the inverse transport of FITC-dextran 20 kDa, from basolateral to apical side was tested as shown in Figure 3.2. D. Once again, a constant difference between the two inserts was observed throughout the assay. Even though both described rising in the amount of dextran over time, the CVM showed a higher amount than PET. Interestingly, both types of transwells reached a flat curve after 45 min with minimal changes afterwards. The maximum concentrations were 0.2408 ± 0,01358 mg in the CVM transwells and 0,04988 ± 0.002138 mg in the PET.

Generally speaking, throughout these assessments, the CVM by Kanto demonstrated a higher permeability to FITC-dextran, regardless of its molecular mass, than PET by Costar. While the CVM transwells showed a similar transported

amount of FITC-dextran from the apical to the basolateral side and vice versa, the PET resulted in an increased diffusion from the basolateral to apical part compared to its counterflow.

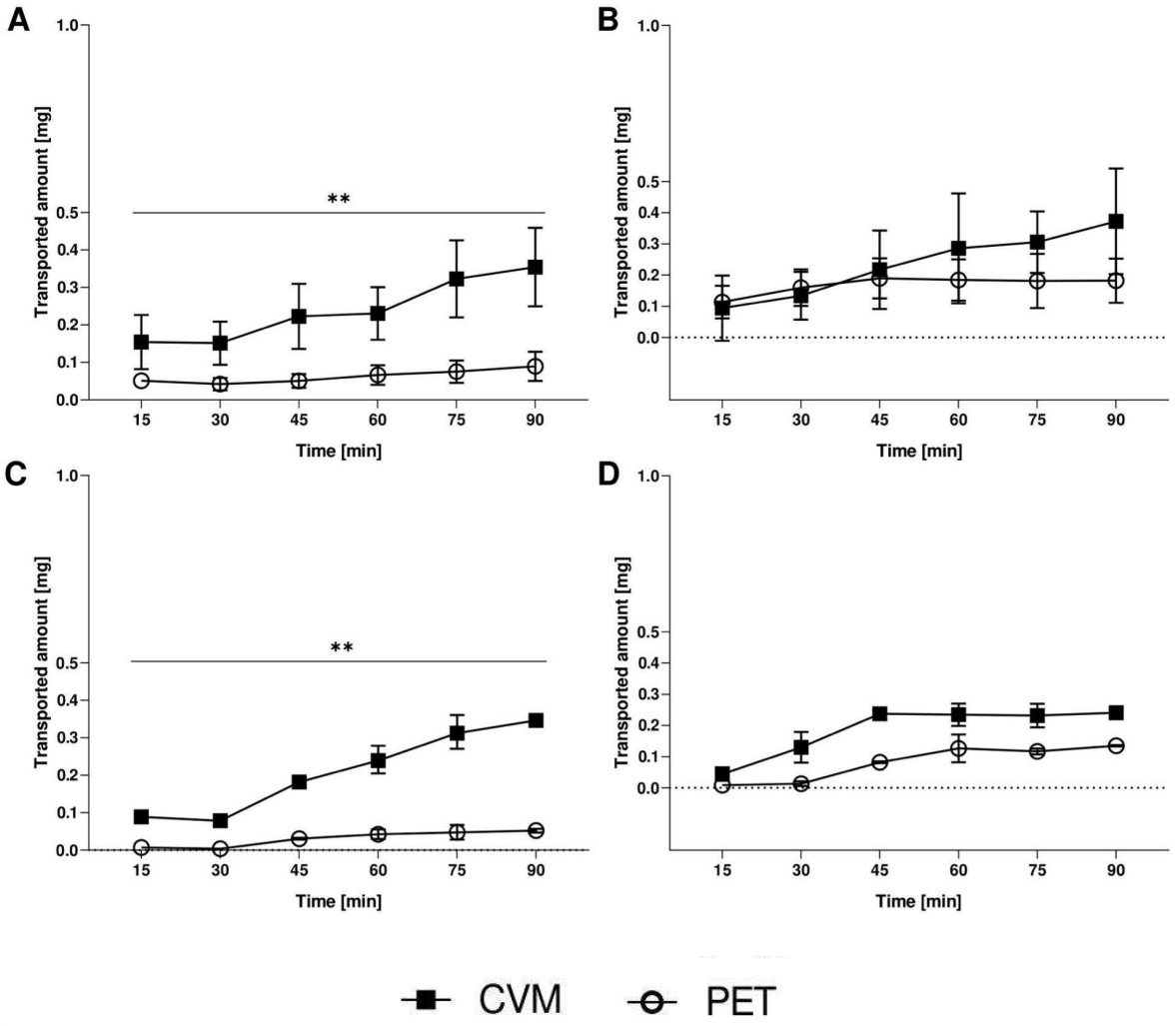

Figure 3.2. Permeability Study. (A) Time course of FITC-Dextran 4 kDa from apical to basolateral side (ab). (B) Time course of FITC-Dextran 4 kDa from basolateral to apical side (ba). (C) Time course of FITC-Dextran 20 kDa from apical to basolateral side (ab). (D) Time course of FITC-Dextran 20 kDa from basolateral to apical side (ba). Cells were seeded at a density of 100.000 cells per cm^2. Data show means ± SD; n = 3; statistical significance of ** $p<0.01$.

Thereafter, the rate at which FITC-dextran crossed through the membrane of the transwells was then screened.

Results from the permeability study were considered to determine the apparent permeability coefficient using the equation 2.3 in section 2.4. Thus, the coefficient values were compared in two settings, cell monolayers exposed to FITC-dextran 4 kDa and those exposed to FITC-dextran 20 kDa. Each setting included comparisons between the two types of transwells as well as the transport from the apical to basolateral side and counterflow. Figure 3.3 illustrates the results obtained.

Overall, thePET showed lower permeability coefficient than the CVM. Particularly, the apical to basolateral diffusion of FITC-dextran 4 kDa in PET was statistically significantly lower than CVM inserts (Figure 3.3 A). Apical to basolateral transport and vice versa, resulted in 3.9-fold and 4.1-fold higher P_{app} respectively.

In contrast, a modest difference was observed between the PET and the CVM ones when FITC-dextran 20 kDa was added (Figure 3.3 B). Herein, the lowest coefficient value was depicted in the basolateral to apical side of the PET, with a value of 0,00004017 ± 0,00002438 cm/s, while the CVM recorded almost 1.6-fold higher coefficient. In the apical to basolateral analysis, the P_{app} was slightly higher with a calculated value of 0,00004478 ± 0,0000311 in the PET, almost half the observed in the CVM transwells.

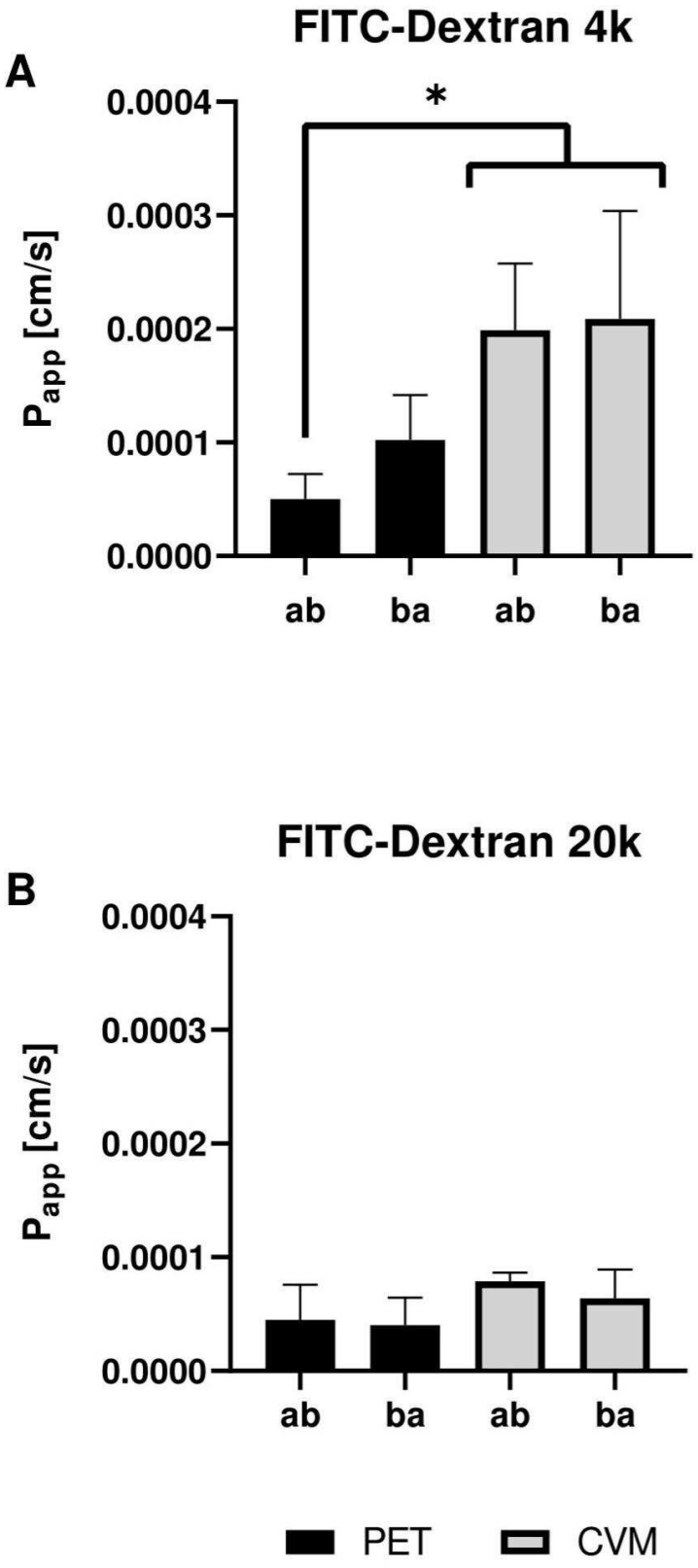

Figure 3.3. Apparent permeability coefficient (P_{app}). Data show means ± SD; n > 3; significant difference is *p<0.05.

3.3. CONFOCAL LASER SCANNING MICROSCOPY

Having in mind the TEER assessment throughout time as well as the characterisation of the monolayer permeability, confocal microscopy was performed. The objective was to determine and compare the assembly of TJ in NCI–H441 cells in both CVM and PET. Thus, cells were fluorescently labelled with anti-ZO-1 antibody conjugated with Alexa Fluor 594 was used to evaluate the assembly of TJ, while nuclei were counterstained with DAPI. Images were obtained on days 3, 6, and 12 and illustrated in Figures 3.5 to 3.10.

Prior to fluorescent-staining, microphotographs were obtained using a phase contrast microscope. As expected, results depicted in Figure 3.4 demonstrated the increasing cell density over time.

Both types of inserts were tested. On day 3 (Figure 3.4 A-B), both CVM and PET showed the ongoing arrangement of the cell monolayer. Though we observed a single layer of cells, there were also other cells fitting into it. In day 6 (Figure 3.4 C-D) uniform cell monolayers were obtained in the two transwell types; the distribution of the cells was homogeneously distributed. In contrast, on day 12, the PET (Figure 3.4 E) showed a very high cell density. Cells changed the usual shape to give space for the growing density while a greater number of detached cells were detected in the media. Additionally in the CVM tranwells (Figure 3.4 F), colony-shape accumulations of cells were observed.

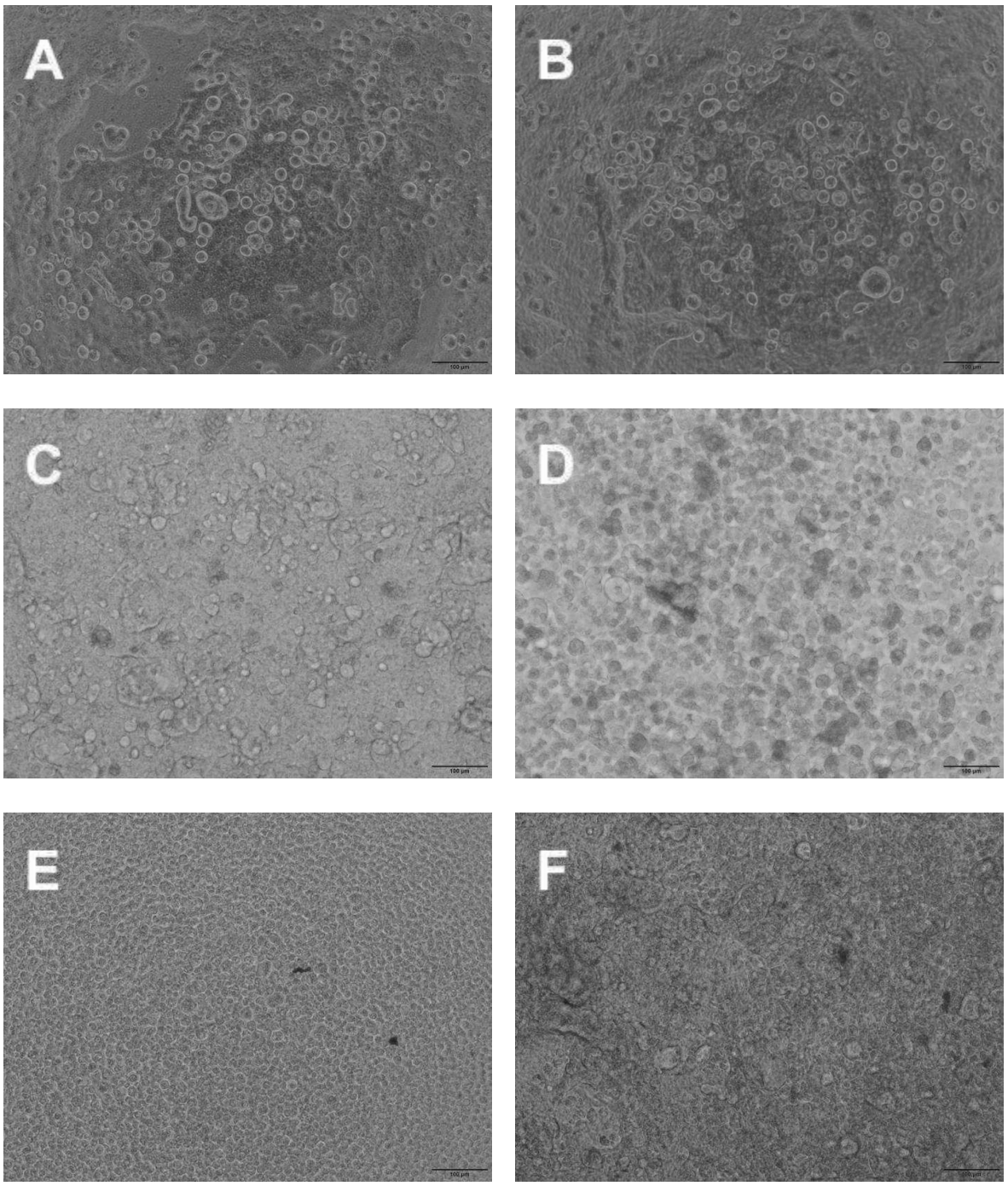

Figure 3.4. Monolayer of H441 cell line on different days. Left: PTE Right: CVM. (A-B) day 3 (C-D) day 6 (E-F) day 12.

Following the evaluation of the monolayer, cells were fluorescently labelled with anti-ZO-1 antibody conjugated with Alexa Fluor 594 to determine the TJ constructs. Nuclei were counterstained with DAPI. Similarly to the previous experiment, microphotographs were obtained on days 3, 6, and 12 and arranged in Figures 3.5 to 3.10.

Firstly, day 3 showed the lowest signal detection out of the experiments carried out in both transwell brands (Figure 3.5 and 3.6). Good signal was detected from DAPI; however, TJ was dispersed and inconsistent.

On the other hand, images from day 6 resulted in the most clear detection of TJ in both CVM and PET (Figure 3.7 and 3.8). Herein, the TJ represented by an intense colour red was homogeneous and clearly outlined the cell-to-cell constructs. Additionally, the images confirm the uniform cell distribution observed previously with the phase contrast microscope and also confirmed by the DAPI staining.

Finally, on day 12, although the TJ were clearly present, the two types of inserts illustrated a rather diffuse signal. Single cells were difficult to detect as interrupted cell outlines were observed (Figure 3.9 - 3.10). Generally speaking, a slightly higher number of cells were detected in the PET (Figure 3.9).

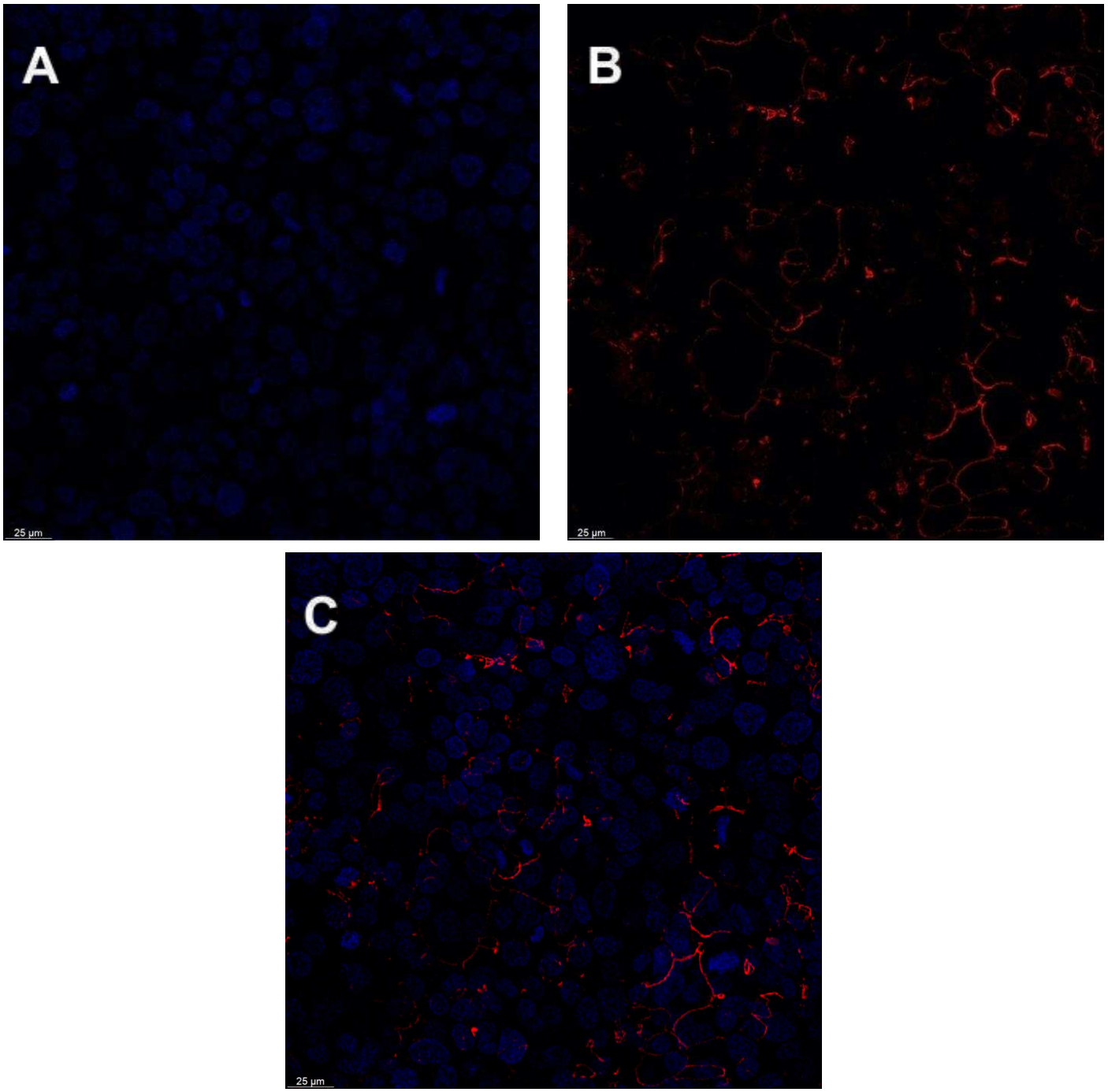

Figure 3.5. CLSM of NCI-H441 on PET imaged on day 3. (A) Staining of the nucleus with DAPI (B) Staining of the ZO-1 proteins with rabbit monoclonal anti- ZO-1 Ab (C) merged picture.

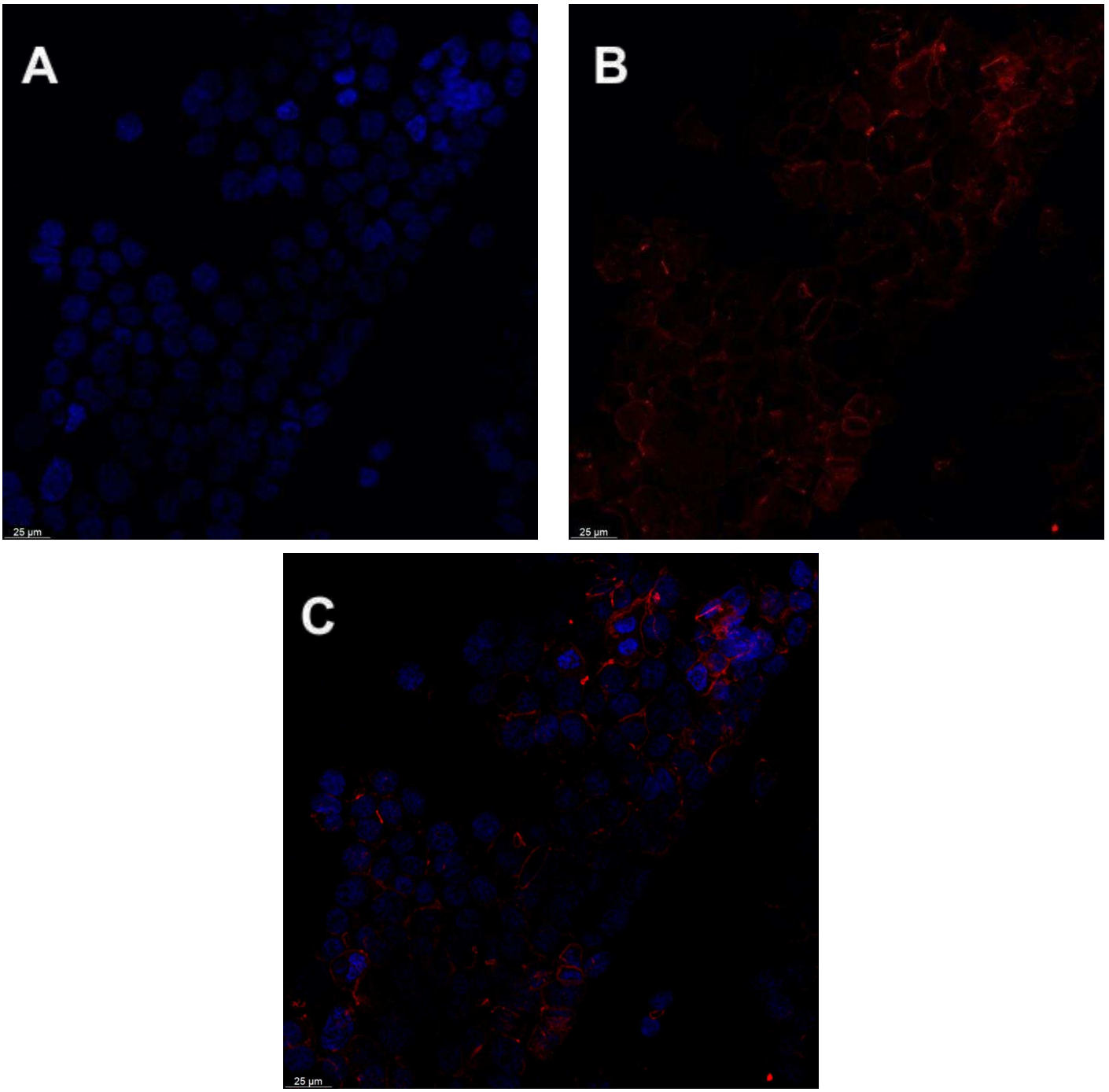

Figure 3.6. CLSM of NCI-H441 on CVM imaged on day 3. (A) Staining of the nucleus with DAPI (B) Staining of the ZO-1 proteins with rabbit monoclonal anti-ZO-1 Ab (C) merged picture.

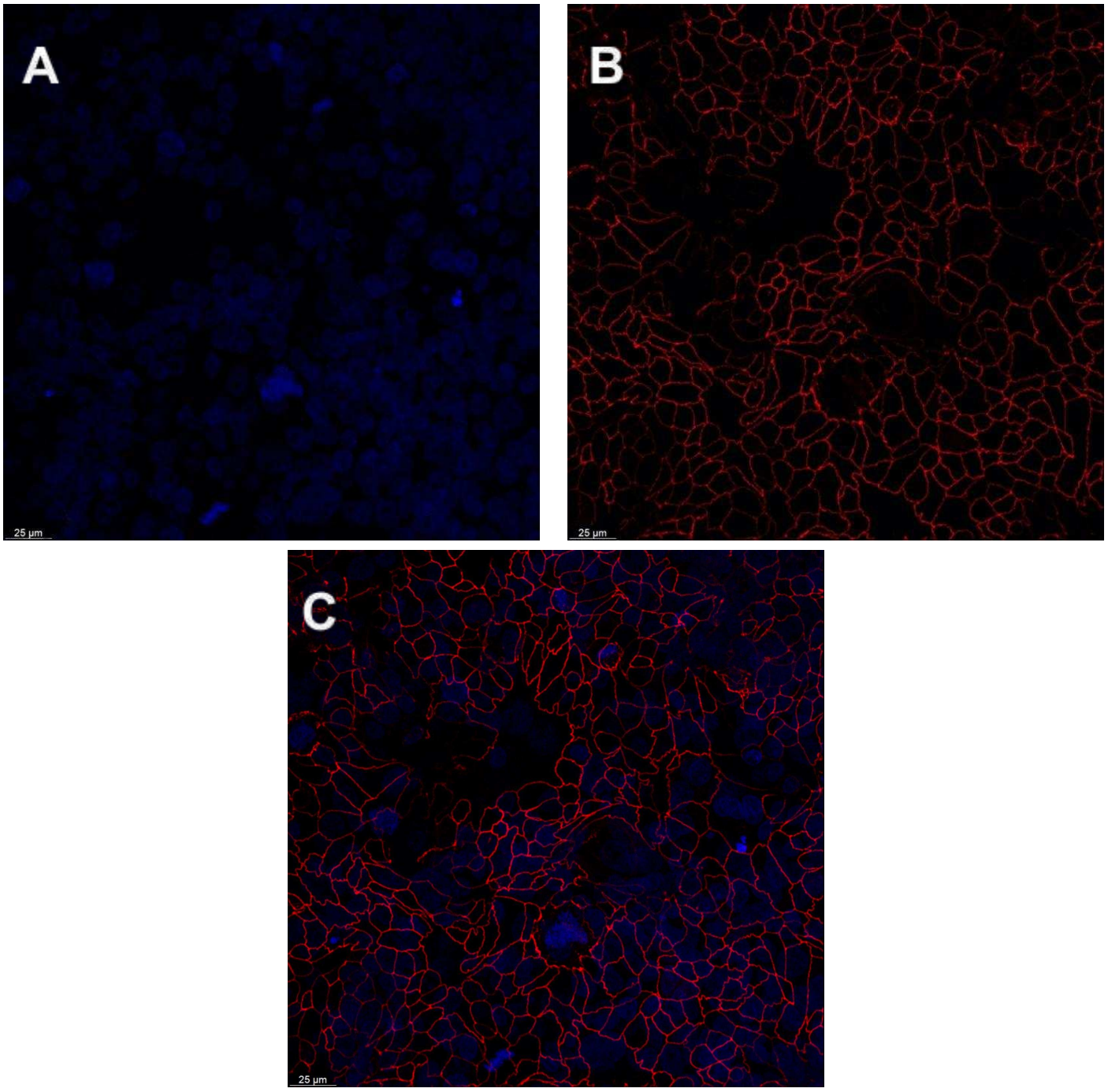

Figure 3.7. CLSM of NCI-H441 on PET imaged on day 6. (A) Staining of the nucleus with DAPI (B) Staining of the ZO-1 proteins with rabbit monoclonal anti- ZO-1 Ab (C) merged picture.

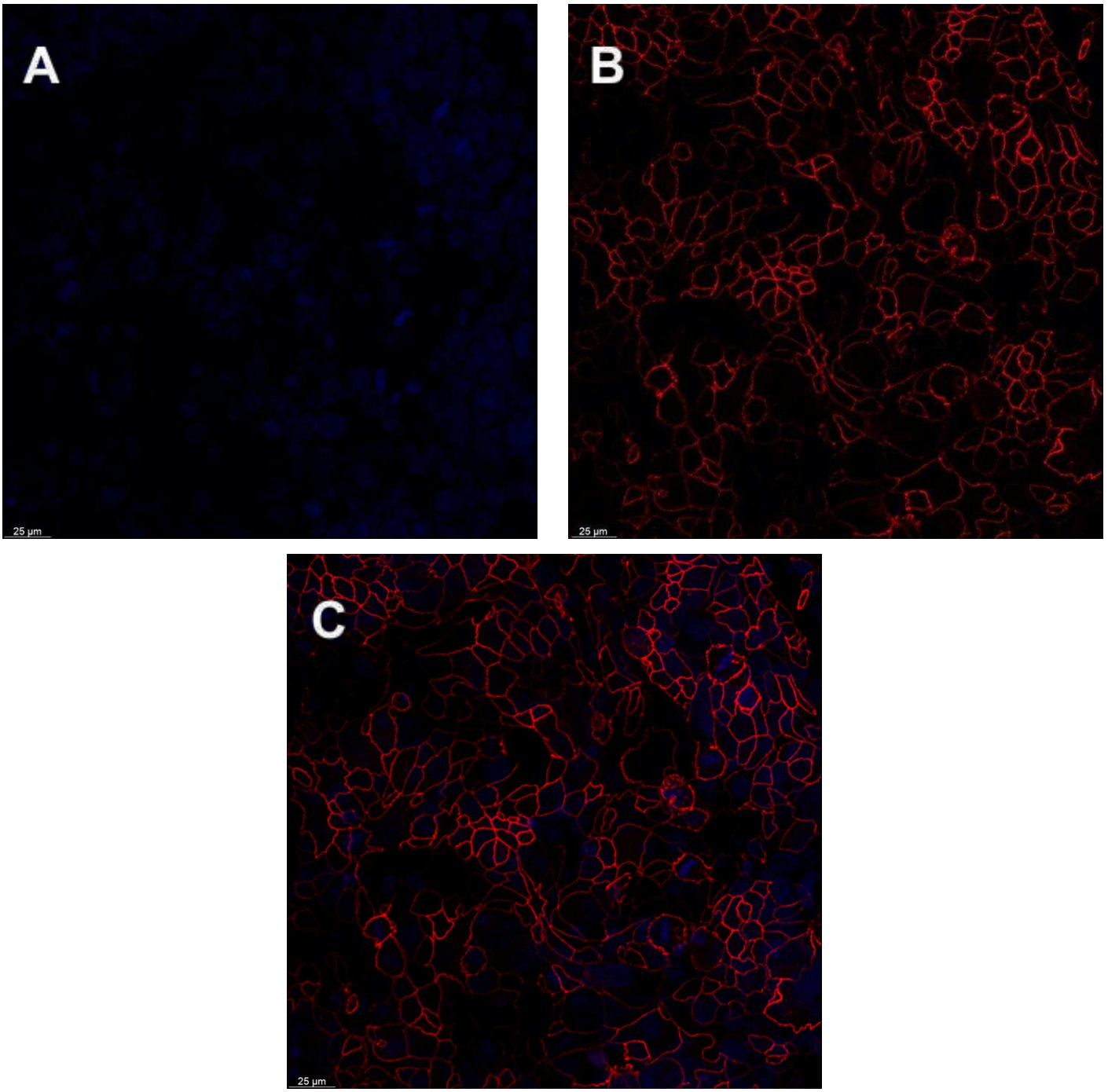

Figure 3.8. CLSM of NCI-H441 on CVM imaged on day 6. (A) Staining of the nucleus with DAPI (B) Staining of the ZO-1 proteins with rabbit monoclonal anti-ZO-1 Ab (C) merged picture.

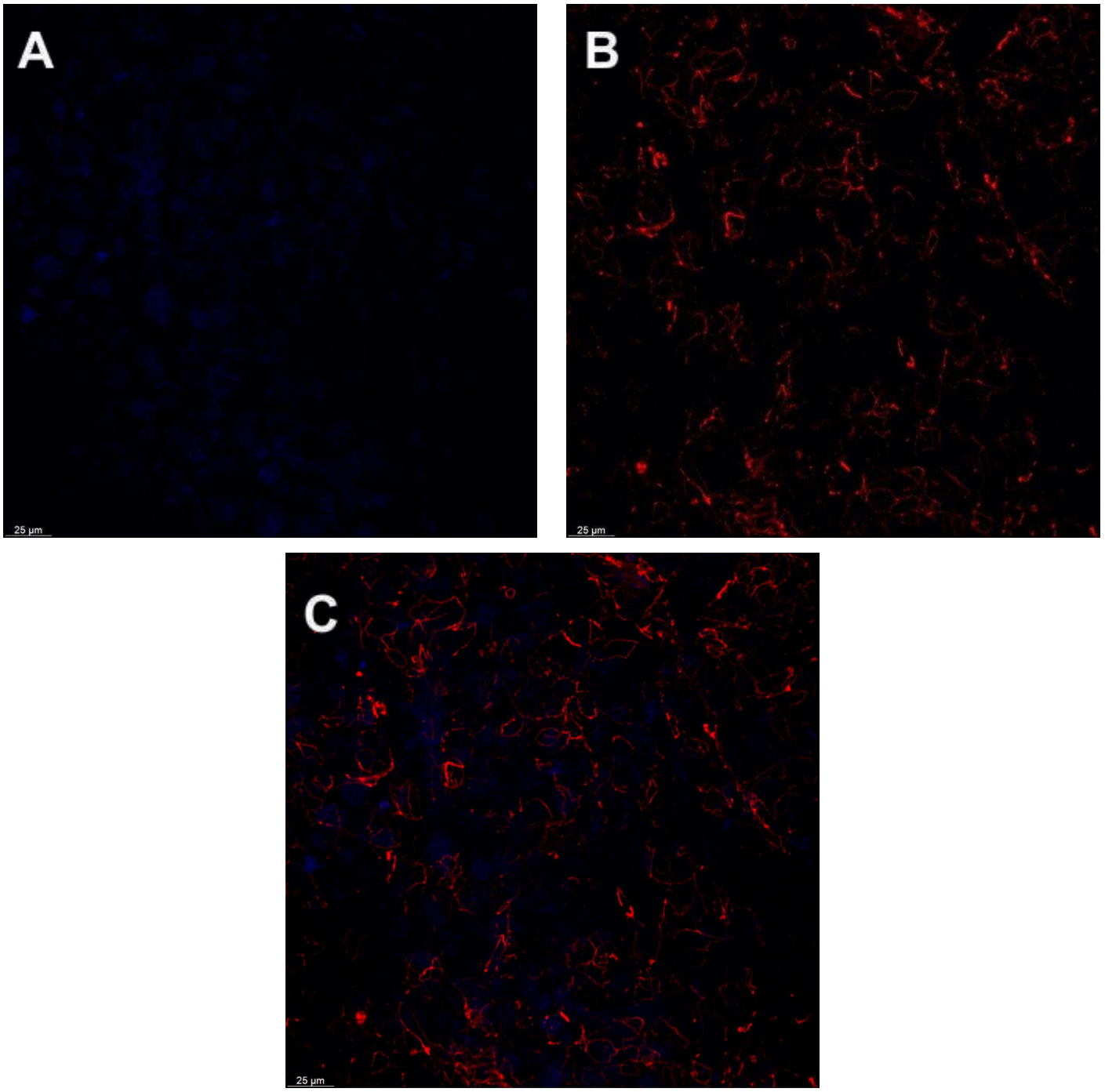

Figure 3.9. CLSM of NCI-H441 on PET imaged on day 12. (A) Staining of the nucleus with DAPI (B) Staining of the ZO-1 proteins with rabbit monoclonal anti-ZO-1 Ab (C) merged picture.

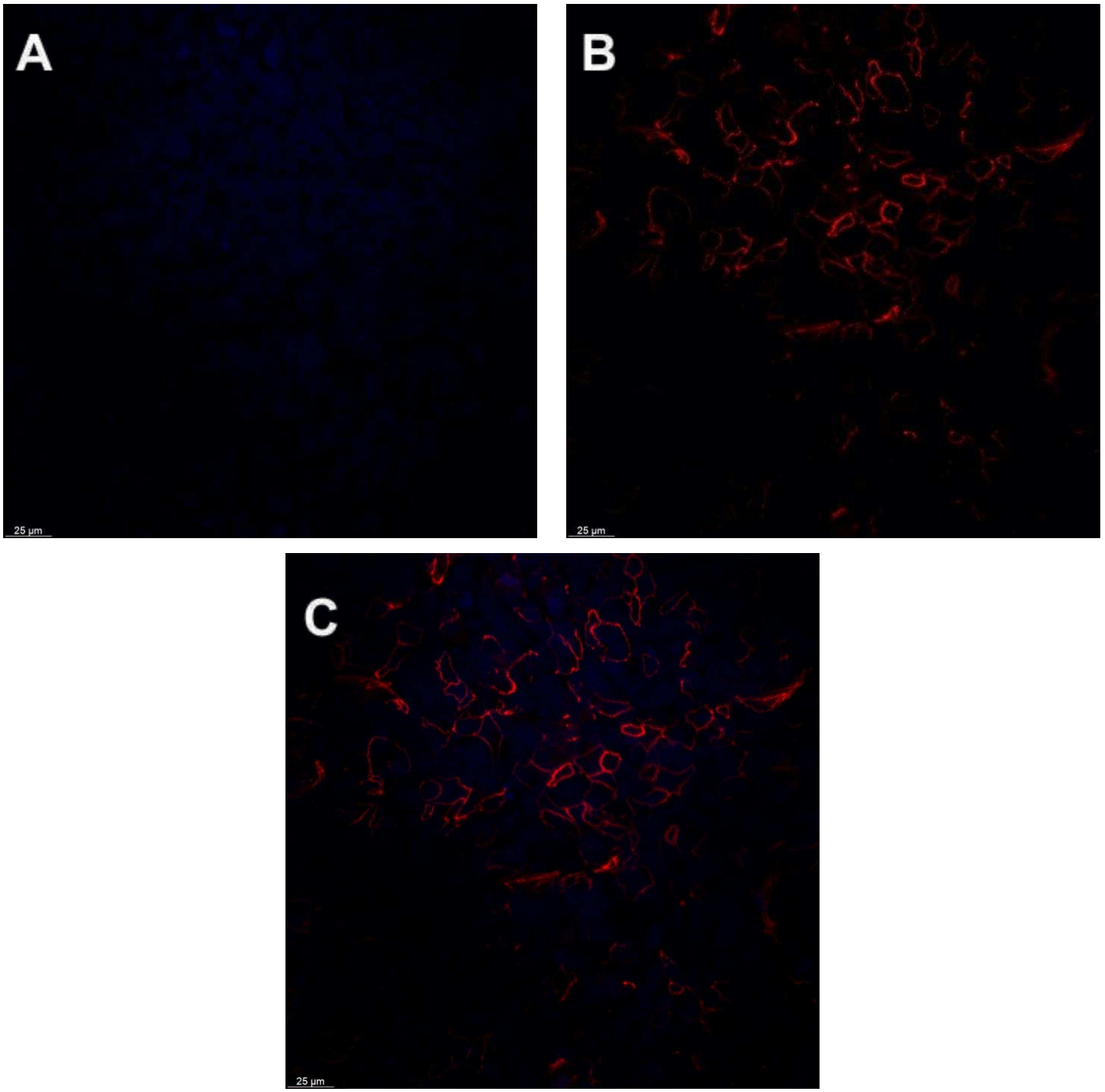

Figure 3.10. CLSM of NCI-H441 on CVM imaged on day 12. (A) Staining of the nucleus with DAPI (B) Staining of the ZO-1 proteins with rabbit monoclonal anti-ZO-1 Ab (C) merged picture.

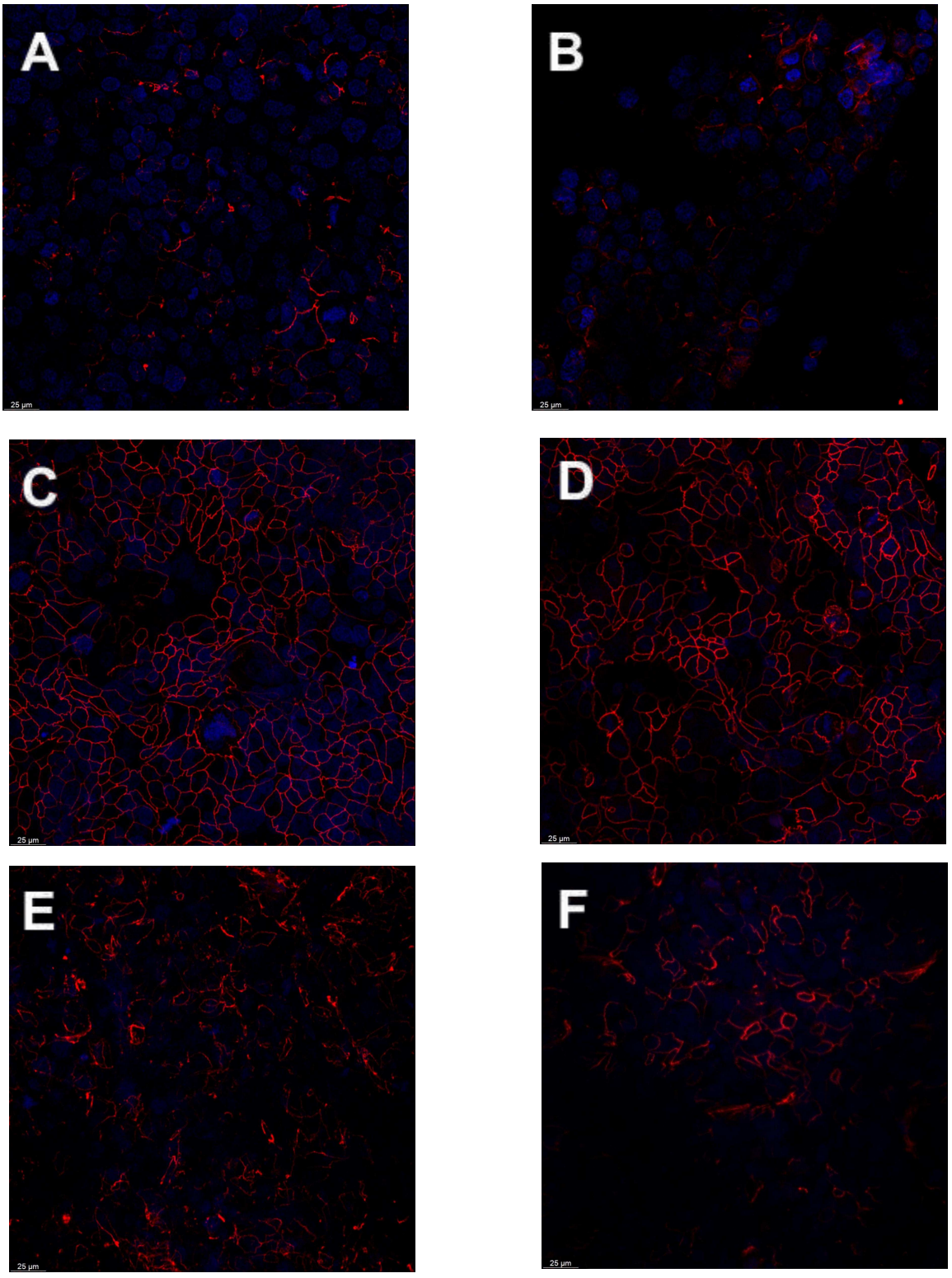

Figure 3.11. Overview of merged CLSM images on the different days. Left: PET.Right: CVM. (A-B) day 3 (C-D) day 6 (E-F) day 12

CHAPTER 4:

DISCUSSION

The non-invasive [28] TEER analysis is a well established and widely used method to quantitatively evaluate the integrity of TJ in cell membranes [29], [30]. Due to the strong correlation of TEER levels to the uniformity of the cell monolayer, frequently, TEER assessments are performed before transport studies [28]. Furthermore, an important advantage of TEER analysis is the feasibility to collect real-time measurements without damaging the cells and minimal to non environment disturbance [28]. This is due to the frequency, as low as 12.5 Hz, created by the epithelial voltohmmeter (EVOM) and passed on to the chopsticks [28] . By placing the chopsticks in the medium of the apical and basolateral chambers, alternating current (AC) goes through, and according to Ohm's Law, the voltage of AC equals the resistance multiplied by the transwell's area [30].

Although it was shown that stem and primary cells are not developing functional and tight monolayers *in vitro,* thus no TEER parameters can be detected [31], NCI-H441 cells, in contrast, are commonly used in blood-air barrier models due to their ability to produce reliable TEER values [32]. However, it is important to mention that growth media has to be supplemented with chemical compounds [21] to promote cell proliferation and differentiation, which are associated with higher expression of TJ [7]. In order to reach confluent monolayers, the addition of dexamethasone and ITS is needed [8]. It has been reported that both compounds increase the development of TJ and have a positive influence on the properties of the cell model. Furthermore, glucocorticoids enhance the stability and function of TJ. Reports suggest that this improvement could be due to the regulation of claudin-8 [32]. Additionally, it was demonstrated by Selo et al., that high TEER values are linked to a high mRNA expression of ZO-1 and the claudins 1, 3, 4, and 5 [32].

Salomon et al. reported in 2014, low TEER values of around 100 Ωcm^2 in NCI-H441 cells cultured in LCC or AIC conditions in medium without corticosteroids [21], which supports observations that supplementing medium with steroids could be beneficial when assessing TEER.
Moreover, it was shown that other glucocorticoids such as budesonide and beclomethasone dipropionate could increase the activity of MRP1 in NCI-H441 cells [33]. For this reason glucocorticoids should be chosen accordingly to the studies setting.

Neuhausen et al. reported TEER values of 438 ± 9 Ωcm² in cells seeded on PVDF membranes coated with collagen and under LCC conditions. Hermanns et al. showed NCI-H441 reached values of 218 ± 83 Ωcm² on PC membrane supplied with 1 µM dexamethasone [7], [34].
Recent studies have shown that in addition to supplementing the culture medium with steroids, the seeding density has an impact on the TEER levels. For instance, a seeding density of 250.000 cells per cm^2 could lead to TEER values higher than 1000 Ωcm² on cells seeded in PTE membranes [21], [35].

In this project, the highest TEER recordings were found on day 7, which directly correlates with the confluency peak observed in cultures, depicting 152 ± 36.50 Ωcm^2 for PET and 197.7 ± 20.44 Ωcm^2 for CVM (Figure 3.1.); a difference between the two membranes of around 45 Ωcm^2. A similar trend of higher TEER values in CVM over PET was also observed in human microvascular endothelial cells (HMVEC).

An increment of 22 Ωcm^2 for CVM than PET membrane was shown. TEER values for the blank membrane were equal in both cases [36]. A reason for higher TEER values using the same growth supplements and cell line, could be the properties of CVM. The high density collagen membrane has a similar character as the connective tissue *in vivo*, providing more suitable conditions for cell growth than PET [37].

Anyway, TEER results of this thesis being lower than reported in studies of the last years can be due to different seeding densities and dexamethasone concentration [21]. Passaging number and temperature can also influence the TEER value. A high passage number can decrease TJ expression, leading to low TEER values. The temperature instead can change the outcome of the reading, a 20 - 30 min on RT should prevent TEER artefacts [28], [31].
Furthermore the values depend also on the correct handling of the chopsticks (electrodes). An incorrect handling, as not covering both electrodes with fluid, holding the chopsticks in another angle as 90° can alternate the reading. Moreover,

due to electrochemical corrosion after several usages the electrodes could not function properly [31].

Due to the effect of the above mentioned factors, it is important to take them in consideration while comparing TEER values from different studies [38].

Another method for assessing barrier function is the permeability study of the cell monolayer. Those studies are widely used to predict drug permeability through a cell barrier [39]. Different molecules with different molecular weights are used for determining the size selectivity and porosity of the TJ [40].
P_{app} shows the amount of dextran transported per time across the barrier and it is proportional to the membrane permeation [36], [39]. Studies defined a tight barrier to have a P_{app} for 4-10kDa in a range of 10^{-6} to 10^{-8} cm/s [41].
P_{app} for NCI-H441 cells have been found to be 1.5×10^{-7} cm/s for 4kDa FITC dextran with TEER around 500 Ω cm^2 [21].

The results found in the assessment of this thesis showed P_{app} values higher than referred in other studies [21], [41], with CVM having more permeability than PET membrane. As Benson et al. reported, the higher permeability is a characteristic of CVMs [29].

During this thesis a statistical difference was found between 4kDa FITC dextran study, none for the 20kDa. This shows what Turksen demonstrated, that 4kDa FITC dextran has a higher sensitivity of characterising barrier integrity, than other molecular weights [37]. Furthermore, there is a difference of transportation between molecule sizes, showing a tendency of bigger molecules to have a lower permeability rate than smaller molecules [42].

Anyway a consistency between membranes during TEER and permeability studies is found, due to the fact that high P_{app} correlates with lower TEER values. Furthermore, an expression of TJ observed with CLSM was found to be equal in both membranes. CVM and PET did not show a continuous statistical difference throughout the project. Mentionable is that CVM are prompter to be used for assessing monolayer integrity, PET instead show a better usage for permeability studies.

CHAPTER 5:

CONCLUSION AND FUTURE WORK

Over the last years, the research community has shown increasing attention to the development of new *in vitro* alternatives that can better predict future *in vivo* outcomes. Likewise, great efforts are now focusing on improving current technologies while reducing costs.

Therefore, in the need of reliable models that can mimic specific biological events that occur in *in vivo* settings, new alternatives of complex *in vitro* models have been developed such as co-culture, 3D cell cultures, and specialised devices.

The work presented in this thesis successfully tested and compared two different material-based membranes, PET and CVM in order to determine their suitability to develop a stable and replicable model for blood air barrier. Thus, lung adenocarcinoma NCI-H441 cells were cultivated in both transwells. During the length of the studies, both inserts showed consistent TEER values associated with the integrity of the cell monolayer and directly proportional to the cell confluency observed with phase contrast imaging. Such values not only agreed to other scientific reports, but also, were confirmed with microphotographs obtained from confocal laser scanning microscopy techniques. Additionally, using a fluorescently-labelled polymer to determine the permeability of the monolayers, the two membranes depicted high permeability. Nonetheless, CVM technology demonstrated a slightly higher permeability than that observed in PET membranes. Thus, these results can be taken into consideration when CVM inserts are to be used in permeability evaluations.

This thesis describes a series of studies, analyses, and comparisons that are essential for subsequent evaluation stages and for their use in *in vitro* models. Still, in this project, important issues were detected that would be valuable for further investigation.

The characterisation of the CVM and PET membranes could be investigated more extensively. Additionally, similar experiments to those presented herein could be performed in AIC conditions as a comparative model. Also, the association of the concentrations of dexamethasone and collagen or alternative supplements to the growth rate of cells can be further studied. Finally, co-culture with different relevant

cells could be performed aiming to minimise the gap between these *in vitro* models and in vivo settings.

REFERENCES

[1] D. Bösch, *Lunge und Atemwege*. in Springer-Lehrbuch. Berlin, Heidelberg: Springer Berlin Heidelberg, 2014. doi: 10.1007/978-3-642-28223-2.

[2] J. A. Sake, “EXPLORING MEMBRANE TRANSPORTERS IN LUNG EPITHELIAL CELLS: DRUG–TRANSPORTER INTERACTION ANALYSES IN DIFFERENT *IN VITRO* MODELS,” 2023.

[3] M. A. Selo, “The Role of Drug Transporters in Chronic Obstructive Pulmonary Disease,” 2018.

[4] C. Amador, C. Weber, and M. Varacallo, “Anatomy, Thorax, Bronchial.”

[5] Endter S. ‘CHARACTERISATION OF DRUG TRANSPORTERS IN HUMAN RESPIRATORY EPITHELIAL CELLS’- Dissertation 2010.

[6] Salomon J. ‘DRUG TRANSPORT ACROSS THE HUMAN RESPIRATORY EPITHELIAL BARRIER’ Dissertation, 2012.

[7] M. I. Hermanns, R. E. Unger, K. Kehe, K. Peters, and C. J. Kirkpatrick, “Lung epithelial cell lines in coculture with human pulmonary microvascular endothelial cells: development of an alveolo-capillary barrier *in vitro*,” *Lab. Invest.*, vol. 84, no. 6, pp. 736–752, Jun. 2004, doi: 10.1038/labinvest.3700081.

[8] M. A. Selo, J. A. Sake, K.-J. Kim, and C. Ehrhardt, “*In vitro* and ex vivo models in inhalation biopharmaceutical research — advances, challenges and future perspectives,” *Adv. Drug Deliv. Rev.*, vol. 177, p. 113862, Oct. 2021, doi: 10.1016/j.addr.2021.113862.

[9] P. M. Graybill, E. J. Jacobs, A. Jana, A. Agashe, A. S. Nain, and R. V. Davalos, “Ultra-thin and ultra-porous nanofiber networks as a basement-membrane mimic,” *Lab. Chip*, vol. 23, no. 20, pp. 4565–4578, 2023, doi: 10.1039/D3LC00304C.

[10] C. Ehrhardt and K. Kim, *Drug absorption studies: in situ, in vitro and in silico models*. New York: Springer, 2008.

[11] K. Matter and M. S. Balda, “Functional analysis of tight junctions,” *Epithel. Polarity Morphog.*, vol. 30, no. 3, pp. 228–234, Jul. 2003, doi: 10.1016/S1046-2023(03)00029-X.

[12] K. Brune, J. Frank, A. Schwingshackl, J. Finigan, and V. K. Sidhaye, “Pulmonary epithelial barrier function: some new players and mechanisms,” *Am. J. Physiol.-Lung Cell. Mol. Physiol.*, vol. 308, no. 8, pp. L731–L745, Apr. 2015, doi: 10.1152/ajplung.00309.2014.

[13] L. Shen, C. R. Weber, D. R. Raleigh, D. Yu, and J. R. Turner, “Tight junction pore and leak pathways: a dynamic duo,” *Annu. Rev. Physiol.*, vol. 73, pp. 283–309, 2011, doi: 10.1146/annurev-physiol-012110-142150.

[14] C. Zihni, C. Mills, K. Matter, and M. S. Balda, “Tight junctions: from simple barriers to multifunctional molecular gates,” *Nat. Rev. Mol. Cell Biol.*, vol. 17, no. 9, pp. 564–580, Sep. 2016, doi: 10.1038/nrm.2016.80.

[15] H. Li, D. N. Sheppard, and M. J. Hug, “Transepithelial electrical measurements with the Ussing chamber,” *J. Cyst. Fibros.*, vol. 3, pp. 123–126, Aug. 2004, doi: 10.1016/j.jcf.2004.05.026.

[16] J. L. Sporty, L. Horálková, and C. Ehrhardt, “*In vitro* cell culture models for the assessment of pulmonary drug disposition,” *Expert Opin. Drug Metab. Toxicol.*, vol. 4, no. 4, pp. 333–345, Apr. 2008, doi: 10.1517/17425255.4.4.333.

[17] B. Forbes and C. Ehrhardt, “Human respiratory epithelial cell culture for drug delivery applications,” *Eur. J. Pharm. Biopharm. Off. J. Arbeitsgemeinschaft Pharm. Verfahrenstechnik EV*, vol. 60, no. 2, pp. 193–205, Jul. 2005, doi: 10.1016/j.ejpb.2005.02.010.

[18] L. G. Dobbs, M. S. Pian, M. Maglio, S. Dumars, and L. Allen, “Maintenance of the differentiated type II cell phenotype by culture with an apical air surface,” *Am. J. Physiol.-Lung Cell. Mol. Physiol.*, vol. 273, no. 2, pp. L347–L354, Aug. 1997, doi: 10.1152/ajplung.1997.273.2.L347.

[19] K. J. Kim, Z. Borok, and E. D. Crandall, “A useful *in vitro* model for transport studies of alveolar epithelial barrier,” *Pharm. Res.*, vol. 18, no. 3, pp. 253–255, Mar. 2001, doi: 10.1023/a:1011040824988.

[20] B. Forbes, “Human airway epithelial cell lines for *in vitro* drug transport and metabolism studies,” *Pharm. Sci. Technol. Today*, vol. 3, no. 1, pp. 18–27, Jan. 2000, doi: 10.1016/S1461-5347(99)00231-X.

[21] J. J. Salomon *et al.*, “The cell line NCI-H441 is a useful *in vitro* model for transport studies of human distal lung epithelial barrier,” *Mol. Pharm.*, vol. 11, no. 3, pp. 995–1006, Mar. 2014, doi: 10.1021/mp4006535.

[22] “Transwell® Permeable Supports | Guidelines for Use | Corning.” Accessed: May 31, 2024. [Online]. Available: https://www.corning.com/worldwide/en/products/life-sciences/products/permeable-supports/transwell-guidelines.html

[23] 技術関東化学株式会社, 伊勢原研究所開発本部, and 宏之山口, “ad-MEDビトリゲル®とその創薬,化学物質安全性試験への応用”.

[24] M. Uzu and T. Takezawa, “Novel microvascular endothelial model utilizing a collagen vitrigel membrane and its advantages for predicting histamine-induced microvascular hyperpermeability,” *J. Pharmacol. Toxicol. Methods*, vol. 106, p. 106916, Nov. 2020, doi: 10.1016/j.vascn.2020.106916.

[25] Accessed: May 27, 2024. [Online]. Available: https://www.kanto.co.jp/english/products/life_science/cellculture/ad-MED_01.html

[26] T. Takezawa, K. Ozaki, A. Nitani, C. Takabayashi, and T. Shimo-Oka, “Collagen vitrigel: a novel scaffold that can facilitate a three-dimensional culture for reconstructing organoids,” *Cell Transplant.*, vol. 13, no. 4, pp. 463–473, 2004, doi: 10.3727/000000004783983882.

[27] “3470 | 6.5 mm Transwell® with 0.4 µm Pore Polyester Membrane Insert, Sterile | Corning.” Accessed: May 27, 2024. [Online]. Available: https://ecatalog.corning.com/life-sciences/b2b/ME/en/Permeable-Supports/Inserts/Transwell%C2%AE-Clear-Inserts%2C-Polyester-%28PET%29-membrane/p/3470

[28] B. Srinivasan, A. R. Kolli, M. B. Esch, H. E. Abaci, M. L. Shuler, and J. J. Hickman, “TEER Measurement Techniques for *In Vitro* Barrier Model Systems,” *SLAS Technol.*, vol. 20, no. 2, pp. 107–126, Apr. 2015, doi: 10.1177/2211068214561025.

[29] K. Benson, S. Cramer, and H.-J. Galla, “Impedance-based cell monitoring: barrier properties and beyond,” *Fluids Barriers CNS*, vol. 10, no. 1, p. 5, Jan. 2013, doi: 10.1186/2045-8118-10-5.

[30] D. W. Powell, “Barrier function of epithelia,” *Am. J. Physiol.-Gastrointest. Liver Physiol.*, vol. 241, no. 4, pp. G275–G288, Oct. 1981, doi: 10.1152/ajpgi.1981.241.4.G275.

[31] A. Doryab *et al.*, “A Biomimetic, Copolymeric Membrane for Cell‐Stretch Experiments with Pulmonary Epithelial Cells at the Air‐Liquid Interface,” *Adv. Funct. Mater.*, vol. 31, no. 10, p. 2004707, Mar. 2021, doi: 10.1002/adfm.202004707.

[32] M. A. Selo, J. A. Sake, K.-J. Kim, and C. Ehrhardt, “*In vitro* and ex vivo models in inhalation biopharmaceutical research — advances, challenges and future perspectives,” *Adv. Drug Deliv. Rev.*, vol. 177, p. 113862, Oct. 2021, doi: 10.1016/j.addr.2021.113862.

[33] M. A. Selo *et al.*, “Tobacco Smoke and Inhaled Drugs Alter Expression and Activity of Multidrug Resistance-Associated Protein-1 (MRP1) in Human Distal Lung Epithelial Cells *in vitro*,” *Front. Bioeng. Biotechnol.*, vol. 8, p. 1030, Sep. 2020, doi: 10.3389/fbioe.2020.01030.

[34] W. Neuhaus *et al.*, “Lung endothelial cells strengthen, but brain endothelial cells weaken barrier properties of a human alveolar epithelium cell culture model,” *Differentiation*, vol. 84, no. 4, pp. 294–304, Nov. 2012, doi: 10.1016/j.diff.2012.08.006.

[35] E. Schwagerus *et al.*, “Expression and function of the epithelial sodium channel δ-subunit in human respiratory epithelial cells *in vitro*,” *Pflüg. Arch. - Eur. J. Physiol.*, vol. 467, no. 11, pp. 2257–2273, Nov. 2015, doi: 10.1007/s00424-015-1693-5.

[36] M. Uzu and T. Takezawa, “Novel microvascular endothelial model utilizing a collagen vitrigel membrane and its advantages for predicting histamine-induced microvascular hyperpermeability,” *J. Pharmacol. Toxicol. Methods*, vol. 106, p. 106916, Nov. 2020, doi: 10.1016/j.vascn.2020.106916.

[37] K. Turksen, *Permeability barrier: methods and protocols*. in Methods in molecular biology, no. 2367. New York: Humana Press, 2021.

[38] J. Yeste, X. Illa, M. Alvarez, and R. Villa, “Engineering and monitoring cellular barrier models,” *J. Biol. Eng.*, vol. 12, no. 1, p. 18, Dec. 2018, doi: 10.1186/s13036-018-0108-5.

[39] I. Hubatsch, E. G. E. Ragnarsson, and P. Artursson, “Determination of drug permeability and prediction of drug absorption in Caco-2 monolayers,” *Nat. Protoc.*, vol. 2, no. 9, pp. 2111–2119, Sep. 2007, doi: 10.1038/nprot.2007.303.

[40] S. Bayat *et al.*, “*In vivo* measurement of lung capillary-alveolar macromolecule permeability by saturation bronchoalveolar lavage,” *Crit. Care Med.*, vol. 28, no. 8, 2000, [Online]. Available: https://journals.lww.com/ccmjournal/fulltext/2000/08000/in_vivo_measurement_of_lung_capillary_alveolar.42.aspx

[41] A. Doryab and O. Schmid, “Towards a gold standard functional readout to characterize *In Vitro* lung barriers,” *Eur. J. Pharm. Sci.*, vol. 179, p. 106305, Dec. 2022, doi: 10.1016/j.ejps.2022.106305.

[42] A. Thomas *et al.*, “Characterization of vascular permeability using a biomimetic microfluidic blood vessel model,” *Biomicrofluidics*, vol. 11, no. 2, p. 024102, Mar. 2017, doi: 10.1063/1.4977584.

ABSTRACT

Trotz wichtiger Fortschritte in den letzten Jahren bleiben die Herausforderungen bei der Entwicklung eines zuverlässigen In-vitro-Modells, das die komplexe Umgebung der menschlichen Lunge nachahmen kann, ungelöst. Es besteht ein dringender Bedarf eines solchen Modelles, um eine bessere Vorhersage der pulmonalen Arzneimittelverabreichung zu ermöglichen und gleichzeitig den Einsatz von Tierversuchen zu reduziert.

Um den Erfolg neuer, auf die Lunge abzielender Therapien zu verbessern, präsentiert diese Arbeit einen detaillierten Vergleich von Polyethylenterephthalat (PET)- und Kollagen-Vitrigel-Membranen für die Zellkultur.

Hierin wurde der transepitheliale elektrische Widerstand (TEER) durchgeführt, um die Integrität der Zellmonoschicht zu beurteilen, die für die Entwicklung von Tight Junctions (TJ) von entscheidender Bedeutung ist. Darüber hinaus wurde die Permeabilität der Zellmonoschicht unter Verwendung von FITC-markiertem Dextran mit zwei unterschiedlichen Molekularmassen bewertet, um die Transporteigenschaften der Membranen zu untersuchen. Schließlich wurde die zelluläre Konfluenz jeden Tag mithilfe einer Kontrastphasenmikroskopie aufgezeichnet und mit konfokalen Bildgebungstechniken bestätigt, um das Vorhandensein von TJ festzustellen. Insgesamt erwiesen sich beide verglichenen Membranen als geeignet für die Entwicklung von Blut-Luftbarriere-Modellen.

Die hier vorgestellten Ergebnisse unterstreichen den Vergleich zweier Membranen auf unterschiedlicher Materialbasis und ihre Fähigkeit, unter Verwendung von Alveolarepithelzellen dichte Monoschichten zu erzeugen.